



Universiteit  
Leiden

The Netherlands

## **Dynamics and regulation of the oxidative stress response upon chemical exposure**

Bischoff, L.J.M.

### **Citation**

Bischoff, L. J. M. (2022, January 12). *Dynamics and regulation of the oxidative stress response upon chemical exposure*. Retrieved from <https://hdl.handle.net/1887/3249612>

Version: Publisher's Version

License: [Licence agreement concerning inclusion of doctoral thesis in the Institutional Repository of the University of Leiden](#)

Downloaded from: <https://hdl.handle.net/1887/3249612>

**Note:** To cite this publication please use the final published version (if applicable).

# 3

---

## Screening the microRNA landscape of Nrf2 pathway modulation identifies miR-6499-3p as a novel modulator of the anti-oxidant response through targeting of KEAP1

---

Luc J.M. Bischoff<sup>1</sup>, Nanette G. Vrijenhoek<sup>1</sup>, Johannes P. Schimming<sup>1</sup>, Anke H.W. Essing<sup>1</sup>,  
Lukas S. Wijaya<sup>1</sup>, Jan P. Langenberg<sup>2</sup>, Daan Noort<sup>2</sup>, Bob van de Water<sup>1</sup>

<sup>1</sup> Division of Drug Discovery and Safety, Leiden Academic Centre for Drug Research, Leiden University, Leiden, The Netherlands

<sup>2</sup> Department of CBRN Protection, TNO Defence, Safety and Security, Rijswijk, The Netherlands

**Manuscript in preparation**

## ABSTRACT

The Keap1/Nrf2 anti-oxidant response pathway is of critical importance for the adaptive cell physiology during both (patho)-physiological circumstances and exposure to xenobiotics. The Nrf2 pathway is controlled by various kinases, ubiquitinases and transcriptional co-regulators. So far, a systematic analysis of the functional role of all known microRNAs on the Nuclear factor-erythroid-2-related factor 2 (Nrf2) pathway is lacking. Here we screened a panel of ~2600 individual microRNA mimics for modulation of Nrf2 pathway activation using an endogenous Nrf2 target *Srxn1*-GFP HepG2 reporter cell line in combination with high throughput live confocal imaging after treatment with CDDO-Me. We identified a panel of 16 microRNAs that enhance (including miR-3165, miR-1909-3p, miR-1293, and miR-6499-3p) and 10 microRNAs that inhibit (including miR-200a-3p, miR-363-3p, miR-502-5p, and miR-25-3p) CDDO-Me-induced *Srxn1*-GFP expression. Overall these microRNAs had minimal effects on the activation of other cellular stress response pathways. Transcriptome analysis demonstrated a direct effect of the candidate inhibiting and enhancing microRNAs on Nrf2 target genes, reflecting the direct effect of Nrf2 and Keap1 depletion, respectively. MicroRNAs with identical seed regions showed a large overlap in differential gene expression. Target prediction models identified miR-6499-3p as a modulator of *KEAP1*. miR-6499-3p suppressed *KEAP1* expression and promoted Nrf2 stability and strongly enhanced *Srxn1*-GFP expression in association with protection against oxidative stress-induced cell death. In conclusion, we identified various microRNAs that control the Nrf2 pathway and which might be relevant biomarkers and/or provide alternative therapeutic modalities to modulate Nrf2 pathway activity in health and disease.

## INTRODUCTION

There is increasing evidence that microRNAs are of critical importance in the modulation of chemical-induced drug responses (Balasubramanian et al. 2020). MicroRNAs (miRNAs or miRs) are small ~22-nt non-coding RNAs (Almeida et al. 2011; Lee et al. 1993; Starega-Roslan et al. 2010) and ~2000 human microRNA sequences have been determined (miRBase release 22). The biogenesis of microRNAs consists of multiple different steps (Hou et al. 2011; Lewis et al. 2003). First, pri-miRNA (primary miRNA transcripts) are transcribed in the nucleus by mainly RNA polymerase II or in some cases polymerase III (Borchert et al. 2006; Lee et al. 2004). Next, these pri-miRNAs are cleaved forming precursor microRNA (pre-miRNA) by microprocessor. This microprocessor complex is formed by DROSHA, a double-stranded RNase III enzyme, and its essential cofactor, the double-stranded RNA (dsRNA)-binding protein DiGeorge syndrome critical region 8 (DGCR8) (Lin and Gregory 2015). The pre-miRNA is transported to the cytoplasm by Exportin-5 and cleaved into an imperfectly double-stranded miRNA by the RNase III protein Dicer. The small RNA duplex generated by dicer is loaded onto an AGO protein (AGO2 being the most important), forming a RNA-Induced Silencing Complex (RISC). In RISC, both ends of the microRNA are protected by AGO proteins making them highly stable.

MicroRNAs regulate gene expression at the post-transcriptional level. The microRNA target sites are typically located on the 3'untranslated region of their target mRNAs. These target sites only need to be partially complementary to the microRNA (Lam et al. 2015), which leads to target mRNA translational repression or degradation (Djuranovic et al. 2012; Filipowicz et al. 2008). MicroRNAs can have 100 target sites per microRNA (Brennecke et al. 2005), and mRNAs can be targeted by more than one microRNA (Peter 2010; Wu et al. 2010). MicroRNAs are involved in many physiological processes including the immune response, metabolism, and development (Hou et al. 2011). Furthermore, microRNAs are involved in toxicological responses and disease (Mendell and Olson 2012) including activation and inhibition of various cellular stress response pathways (Bartoszewska et al. 2013).

A critical cellular stress response pathway is the anti-oxidant Nrf2 pathway, named after its transcription factor nuclear factor erythroid 2-related factor 2 (Nrf2). Under basal conditions Nrf2 is bound in the cytoplasm to two Kelch-like ECH-associated protein 1 proteins (Keum and Choi 2014; Zipper and Mulcahy 2002). Nrf2 consist of seven functional domains (Neh1 – Neh7). Of these domains Neh2 contains seven lysine residues which plays a role in the ubiquitination of Nrf2 (Itoh et al. 1999; Zhang et al. 2004), which facilitates the destruction of Nrf2 via the ubiquitin-26S proteasomal pathway (Kobayashi et al. 2004). Furthermore, Neh2 contains two binding sites which

interact with Keap1. These are the ETGE and DLG motives (McMahon et al. 2006). Binding of reactive oxygen species (ROS) or reactive metabolites to one of the cysteine groups of Keap1 is thought to induce a conformational change in Keap1, resulting in the detachment of Nrf2 of the DLG-motif. As a result, ubiquitination cannot take place. Newly produced Nrf2 translocates to the nucleus where, together with members of the musculoaponeurotic fibrosarcoma (Maf) proteins (MafF, MafG and MafK), it binds to the antioxidant response element (ARE). Binding to the ARE results in the transcription of different cytoprotective genes involved in e.g. glutathione metabolism, phase 2 drug-metabolizing enzymes and antioxidant response proteins as, for example, sulfiredoxin1 (Srxn1), hemoxygenase 1 (Hmox1), and NAD(P)H-quinone oxidoreductase 1 (Nqo1) (Hayes et al. 2010; Zhang and Gordon 2004).

The Nrf2 pathway is critical in health and disease. Ischemic-reperfusion injury leads to strong activation of the Nrf2 pathway in e.g. liver, kidney and heart (Dodson et al. 2019). Xenobiotic exposure leads to the activation of the Nrf2 pathway in various target tissues, including various hepato- and nephrotoxic drugs (Copples et al. 2019; Herpers et al. 2016; Hiemstra et al. 2019; Wink et al. 2018). Therapeutic modulation of the Nrf2 pathway has been an important strategy to protect tissue for detrimental levels of oxidative stress under various pathological circumstances, including CDDO-Me (Cuadrado et al. 2018). Moreover, given the sustained activation of Nrf2 signaling in various types of cancer (Dodson et al. 2019), suppression of Nrf2 activity will be of critical importance to overcome the resistance to various anticancer therapeutics.

The Nrf2 pathway is controlled by various signal transduction components. Protein kinases can modulate both Keap1 and Nrf2 post-translational modification involving PKC and PERK (Baird and Yamamoto 2020). Ubiquitination is critical to modulate Nrf2 degradation and involves the KEAP1-CUL3-RBX1 complex (Baird and Yamamoto 2020). Transcriptional co-activators of the MAF family are critical to modulate Nrf2 transcriptional activity (Yamamoto et al. 2018). More recently various microRNAs including miR-200a were identified that modulate the levels of Nrf2 activity through direct modulation of Nrf2 levels (Cheng et al. 2013). Given the opportunities of microRNAs as candidate (mechanistic) biomarkers and therapeutic modulators, so far a systematic evaluation of the role of microRNAs in the control of Nrf2 signaling is lacking. Here the objective was to systematically uncover the microRNA landscape of Nrf2 pathway modulation through a whole genome microRNA mimic arrayed phenotypic high content imaging screen.

## METHODS

### Reagents

A human miRIDIAN miRNA Mimic Library 19.0 + 21.0 Supplement (2 nmol) was obtained from Dharmacon, USA. Upon arrival, plates were resuspended following the manufacturer's description. MicroRNAs were diluted in 1x siRNA buffer (Dharmacon, USA) to a final concentration of 1  $\mu$ M. 5  $\mu$ L microRNA solution/well (96-well plate) was used giving a final concentration of 50 nM/well. siRNAs were obtained from Dharmacon and resuspended in a similar matter. Interferin (Westburg/PolyPlus, NL) was used as a transfection agent.

The following chemicals were used to induce cellular stress response activation: CDDO-Me (CAS: 218600-53-4) was purchased from Cayman Chemicals, USA. Diethyl maleate (CAS: 141-05-9), tert-butylhydroquinone (CAS: 1948-33-0), etoposide (CAS: 33419-42-0) and tunicamycin (CAS:11089-65-9) were purchased from Sigma-Aldrich, USA and dissolved in 100% dimethyl sulfoxide (CAS: 67-68-5) purchased from Sigma-Aldrich, USA. Antibodies were acquired from Santa Cruz (GAPDH: sc-32233 and Cell Signaling (GFP: #2956).

### Cell culture, microRNA transfection, and immunofluorescence

A human hepatoma HepG2 cell line was obtained from American Type Culture Collection (ATCC<sup>®</sup> HB-8065<sup>™</sup>, Wesel, Germany). Previously, HepG2-GFP reporter cells were developed and characterized for Keap1, Nrf2, Srxn1, Hmox1, p21 and Chop/DDIT3 (Wink et al. 2017). Briefly, cell lines were constructed with green fluorescent protein (GFP) reporter genes located on bacterial artificial chromosomes (BACs) that encode C-terminal GFP-tagged fusion proteins, following 500  $\mu$ g/mL G-418. For more information see (Poser et al. 2008). Cells were grown in Dulbecco's Modified Eagle Medium (DMEM) high glucose, supplemented with 10% (v/v) fetal bovine serum (FBS), 25 U/mL penicillin and 25  $\mu$ g streptomycin. Cells were used for experiments until passage 20.

For experiments, 23,000 cells/well were seeded and transfected in a 96-well plate. 72 h after transfection, cells were exposed to different chemicals. After exposure, the plates were measured making use of confocal microscopy (Figure 1A).

For immunofluorescence analysis of the p62 (SQSTM1) protein, plates containing HepG2-Keap1-GFP cells were used. These cells were transfected with microRNAs for 72 hours and exposed to CDDO-Me (30 nM) for 24 h. After this period, cells were washed with PBS and stained with formaldehyde. For immunofluorescence measurement, fixed cells were permeabilized followed by primary antibody SQSTM1/

p62 staining (D5L7G; Cell Signaling, USA); IgG goat anti mouse linked to Cy-3 was used for secondary staining (Jackson ImmunoResearch, NL). Immunofluorescence was evaluated by confocal microscopy as described below.

### Live confocal imaging

Live cell confocal imaging of GFP reporter HepG2 cells was performed on a Nikon Eclipse Ti confocal microscope equipped with four lasers: 366, 408, 488 and 561 nm. A 20x dry PlanApo VC NA 0.75 with 1x zoom was used. Prior to exposure, Hoechst<sub>33342</sub> 100 ng/mL was added to the wells to stain nuclei and propidium iodide (PI) was added to measure cell death. For miRNA screens images were taken at specific time points; for validation screens live cell imaging was performed for a total period of 24 h with 1 hour time intervals. Microscopy images were further analyzed using Cell Profiler and R to define GFP reporter intensity at the single cell level. The fraction of GFP positive cells was calculated by counting the amount of cells with a GFP-value two times above baseline (DMSO control) level.

### Viability assessment

To further explore the impact of microRNA overexpression on cell viability, HepG2-WT were transfected with miRNAs or siRNA controls for 72 h followed by co-staining with Hoechst 33342 and propidium iodide and then treated with 278 or 600  $\mu$ M nitrofurantoin (CAS: 67-20-9, Sigma Aldrich, #N7878) followed by high content imaging of cytotoxicity as previously described (Schimming et al. 2019).

### Western blot

HepG2-WT cells were seeded 200,000 cells/well and transfected in a 24-well plate. After 72 h cells were exposed to different concentrations of CDDO-Me. Cells were lysed after 7 h with direct lysis buffer (70  $\mu$ L/well, 2x SPB (sample buffer: bromophenol blue solution) lysis buffer + 10%  $\beta$ -mercaptoethanol) and stored at -20°C. Proteins were separated on acrylamide gels (7.5%, 15% for SRXN1) and blotted on PVDF membranes. Membranes were blocked with 5% BSA (bovine serum albumine) in Tris-buffered saline (TBS)/0.05% Tween for 1 h at RT. Staining with antibodies (1:1000) was done overnight at 4°C in 1% BSA in TBS/Tween. After washing the membranes were exposed to HRP (GFP) or Cy-5 (housekeeping gene GAPDH) in 1% BSA in TBS/Tween for 1 h at RT. The membrane was exposed to ECL reagent for 5 minutes followed by immunoluminescence detection with ImageQuant™ LAS 4000 (GE Healthcare). Image analysis was done in imageJ.

### Targeted RNA sequencing and bioinformatics

To determine gene expression changes after microRNA transfection, HepG2-WT (wild type) cells were used. The HepG2-WT cells were plated in 96-well plates (23,000

cells/well) and transfected as described above with selected microRNAs. siKEAP, siNFE2L2/Nrf2, mock control, and medium control were taken along as controls. After 72 h of transfection, wells were washed with 200  $\mu$ L PBS and lysed with 50  $\mu$ L TempO-Seq lysis buffer (BioSpyder, USA) for 5 minutes at room temperature. Lysate plates were sealed and immediately frozen at -80 °C. Experiments were performed as three biological replicates. The lysate plates were shipped on dry ice to Bioclavis (Glasgow, Scotland) followed by whole transcriptome TempO-Seq targeted RNAseq analysis (Yeakley et al. 2017).

Differentially expressed genes ( $p_{adj} < 0.05$ ) were identified by the DESeq2 method (Love et al. 2014) using the therein described R package DESeq2. The mock transfection treatment was used as a control and the cutoff for sample exclusion was a total read count of 100,000. Pathway analysis was performed using IPA (QIAGEN Inc., <https://www.qiagenbioinformatics.com/products/ingenuitypathway-analysis>). Pathway enrichment analysis was performed leveraging the function of TXG-MAPr - PHH platform ([https://txg-mapr.eu/WGCNA\\_PHH/TGGATEs\\_PHH/](https://txg-mapr.eu/WGCNA_PHH/TGGATEs_PHH/) (Callegaro et al. 2021)). The log<sub>2</sub> fold change values obtained from high throughput targeted sequencing (TempO-Seq) was uploaded to the online platform after eliminating probes measuring non-expressed genes (base mean = 0). Additionally, we only selected one probe per gene so that for probes which are measuring the expression of similar genes, we only selected one with the least adjusted p-value per condition. The gene expression values measured from TempO-Seq data were plotted according to the gene network model (modules) within the platform. The eigengene scores (EGS) for each module were calculated based on the z-score derived from the log<sub>2</sub> fold change values of the genes consisting the network (module membership).

For microRNA target prediction, three different databases were used: IPA, mirDB (<http://www.mirdb.org>), (Wong and Wang 2015), and TargetScanHuman version 7.1 ([http://www.targetscan.org/vert\\_71](http://www.targetscan.org/vert_71)) (Agarwal et al. 2015). These sites both use an own bioinformatics algorithm to predict possible microRNA targets. For MiRDB we used a prediction score of >80. For Targetscan we used the cumulative context++ score, which estimates the total repression expected from multiple sites of the same microRNA, for each mRNA target predicted (Riffo-Campos et al. 2016).

## Data analysis

Biological replicates were performed 3 times or more as indicated in the figure legends. Statistical analysis was performed in R. Figures were made in R, and Venn diagrams were made with the online tool Venny2.1 (<http://bioinfogp.cnb.csic.es/tools/venny/index.html>).

## RESULTS

### MicroRNA screen for Nrf2 pathway modulation

Here we systematically screened for microRNAs that affect Nrf2 pathway activation. For this we used the BAC-GFP-Srxn1 HepG2 reporter cells where Srxn1-GFP expression is dependent on Nrf2 activity (Wink et al. 2017). In total we screened the effect of expression of ~2600 individual miRNA mimetics. We used CDDO-Me (30 nM) to induce Nrf2 activation and measured the effect of microRNA expression on GFP-Srxn1 levels after 7 h. Since CDDO-Me-induced Srxn1-GFP expression takes ~4 h for onset we could use the 1 h time point as the miRNA only effect (Figure 1B and C). We observed numerous microRNAs affected Srxn1-GFP at 1 h or 7 h after CDDO-Me treatment. Remarkably, the performance on the effect of various microRNAs was stronger than the effect of siKEAP1 (enhancing Srxn1-GFP induction) and siNFE2L2 (suppressing Srxn1-GFP expression), supporting the likely strong effect of individual microRNAs on Nrf2 signaling. For further studies, we focused on the top 100 overlapping microRNAs at both time points, for both Srxn1-GFP enhancing (Figure 1D) and inhibiting (Figure 1E) microRNAs.

Next, we conducted a secondary screen for three biological replicates to validate the hits found in the primary screen (one biological replicate). We selected in total 134 Srxn1-GFP enhancing microRNAs: the top 100 enhancers found 1 h after exposure and the additional 34 microRNAs found in the top 100 after 7 h CDDO-Me exposure. In addition, we selected the top 100 microRNAs that did inhibit the Srxn1-GFP response after 7 h. Most of the 134 Srxn1-GFP enhancing microRNAs promoted the Srxn1-GFP intensity compared to the mock condition as well as the fraction of Srxn1-GFP positive cells (Figure 2A-D and Suppl. Figure 1). Interestingly, some microRNAs displayed a similar enhancement of Srxn1-GFP response as siKEAP1, including miR-3165, miR-1909-3p, miR-1293, and miR-6499-3p. Furthermore, most of the 100 inhibiting microRNAs used in the secondary screen, led to a lower Srxn1-GFP intensity associated with limited number of Srxn1-GFP positive cells (Figure 2E and F). For some microRNAs the effect on inhibition of CDDO-Me-induced Srxn1-GFP expression was stronger than siNFE2L2, including miR-200a-3p, miR-363-3p, miR-502-5p, and miR-25-3p. For follow up experiments, based on the comparison on the effect of siKEAP1 and siNFE2L2, we selected the top 16 Srxn1-GFP enhancing microRNAs and the top 10 Srxn1-GFP inhibiting microRNAs (Figure 2G and H). We screened for Nrf2 modulating microRNAs using CDDO-Me as a potent pharmacological activator of Nrf2 signaling through its modification of Keap1. To exclude the context dependency of our results, we verified the effect of the candidate microRNAs also in the context of tert-butylhydroquinone (tBHQ; 100  $\mu$ M) and diethyl maleate (DEM; 100  $\mu$ M), two known inducers of the Nrf2 pathway, but with a different mode of action (Casey et

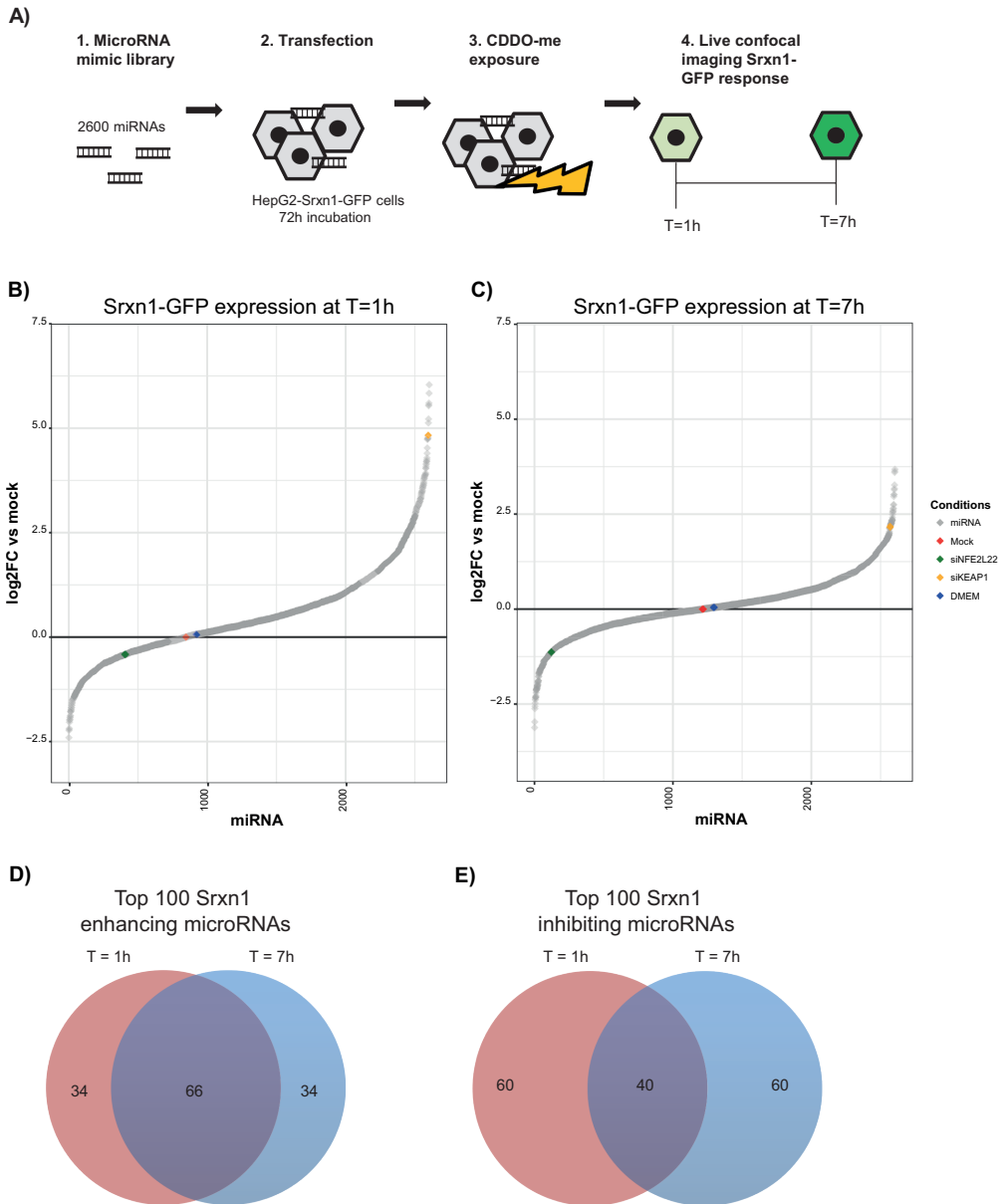


**Figure 1. Systematic screen for microRNA mimetics on Nrf2 activation.**

**A)** Schematic overview of the used *in vitro* method. **B)** Ranked distribution of the microRNAs to their GFP-intensity ( $\log_2FC$  vs mock) 1 h after exposure to 30 nM CDDO-Me. **C)** Ranked distribution of the microRNAs to their GFP-intensity ( $\log_2FC$  vs mock) 7 h after exposure to 30 nM CDDO-Me. **D)** Top 100 Srxn1 enhancing microRNAs for each time point, showing a 66 % overlap between 1 h and 7 h after 30 nM CDDO-Me exposure. **E)** Top 100 Srxn1 inhibiting microRNAs for each time point, showing a 40 % overlap between 1 h and 7 h after 30 nM CDDO-Me exposure.

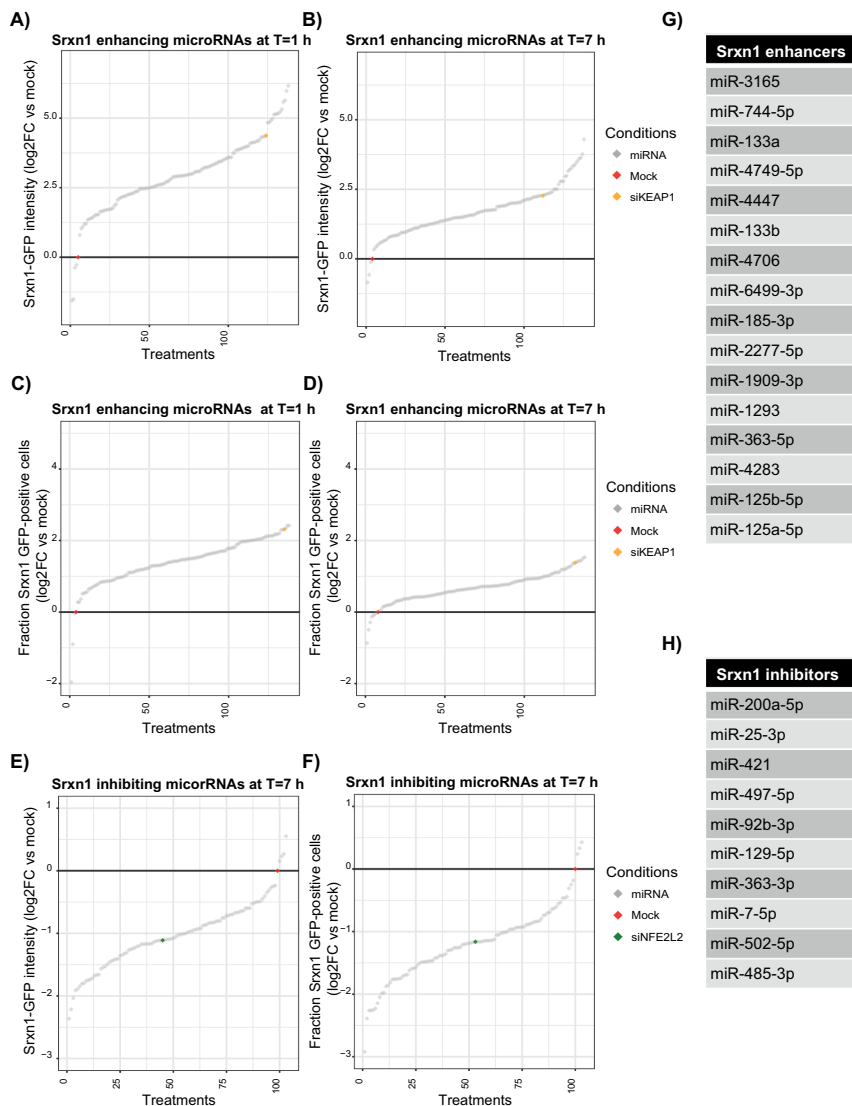


**Figure 2. Validation of candidate Nrf2 signaling modulating microRNAs.**

**A)** Ranked distribution of the 134 selected Srxn1 enhancing microRNAs, including mock and siKEAP1 control, to their Srxn1-GFP intensity (log<sub>2</sub>FC vs mock) after 1 h 30 nM CDDO-Me exposure. **B)** Ranked distribution of the 134 selected Srxn1 enhancing microRNAs, including mock and siKEAP1 control, to their Srxn1-GFP intensity (log<sub>2</sub>FC vs mock) after 7 h 30 nM CDDO-Me exposure. **C)** Ranked distribution of the 134 selected Srxn1 enhancing microRNAs, including mock and siKEAP1 control, to the amount of Srxn1 GFP-positive cells (log<sub>2</sub>FC vs mock) after 1 h 30 nM CDDO-Me exposure. **D)** Ranked distribution of the 134 selected Srxn1 enhancing microRNAs, including mock and siKEAP1 control, to the amount of GFP-positive cells (log<sub>2</sub>FC vs mock) after 7 h 30 nM CDDO-Me exposure. **E)** Ranked distribution of the 100 selected Srxn1 inhibiting microRNAs, including mock and siNFE2L2 control, to their Srxn1-GFP intensity (log<sub>2</sub>FC vs mock) after 7 h 30 nM CDDO-Me exposure. **F)** Ranked distribution of the 100 selected Srxn1 inhibiting microRNAs, including mock and siNFE2L2 control, to the amount of Srxn1 GFP-positive cells (log<sub>2</sub>FC vs mock) after 7 h 30 nM CDDO-Me exposure. **G)** selected Srxn1 enhancing microRNAs. **H)** Selected Srxn1 inhibiting microRNAs.

al. 2002; Priya et al. 2014; Yamauchi et al. 2011, Imhoff and Hansen 2010, Abiko et al 2011, Weber et al 1990) (Suppl. Figure 2).

### Effects of candidate microRNAs on the dynamics of Nrf2 pathway activation

To further increase our understanding of the effect of the selected validated candidate microRNAs on the Nrf2 pathway, we tested the effect of the 16 Srxn1-GFP enhancing and 10 Srxn1-GFP inhibiting microRNAs on Nrf2 activation and Keap1 behavior using our previously established BAC-GFP-Nrf2 and Keap1-GFP HepG2 reporter cell lines. For this we followed the dynamics of the Nrf2-GFP and Keap1-GFP using 24 h live confocal imaging (Figure 3A). We observed strong overall enhancement of Srxn1-GFP activation with some microRNAs already demonstrating Srxn1-GFP expression prior to CDDO-Me addition and with limited enhancement (e.g. miR-6499-3p) or with further strong enhancement of Srxn1-GFP (e.g. miR-4749-5p; Figure 3B). Typically the response of the enhancer was much stronger than for CDDO-Me alone. Interestingly, for some of the enhancing microRNAs, the effect was associated with strongly enhanced Nrf2-GFP nuclear expression levels (e.g. miR-3165; Figure 3C) and was associated with later onset of Keap1-GFP translocation to autophagosome foci (e.g. miR-2277-5p) (Figure 3D and Suppl. Figure 3). Overall, the effect of the validated candidates on the different Nrf2 pathway components was microRNA specific, suggesting different functions of the various microRNAs in modulating the Nrf2 pathway.

### Effects of microRNAs on other generic cellular stress response pathways

MicroRNAs can target multiple genes and therefore potentially affect various cellular stress response pathways. Alternatively, the expression of microRNA mimetics may trigger a general cellular stress response and activate e.g. also an unfolded protein response or the DNA damage response (Figure 4A). Therefore, first we evaluated the effect of the candidate microRNAs on the expression of Hmox1, a stress response gene that is activated upon oxidative stress in various tissues and under the control of AP-1 transcription factors (Medina et al. 2020). While CDDO-Me (30 nM) caused strong activation of the Nrf2-dependent Srxn1-GFP expression, no major induction of Hmox1-GFP was observed. MicroRNAs that did promote Srxn1-GFP induction did not per se affect Hmox1-GFP reporter activation after CDDO-Me treatment, except for miR-2277-5p. Interestingly, miR-485-3p transfection led to a strong Hmox1 activation, irrespective of CDDO-Me treatment (Figure 4B). An explanation for this might be that miR-485-3p is related to the iron-responsive regulation of ferroportin, a cellular iron exporter (Sangokoya et al. 2013). None of the microRNAs caused induction of p21-GFP expression caused by p53 activation, indicating that these microRNAs do

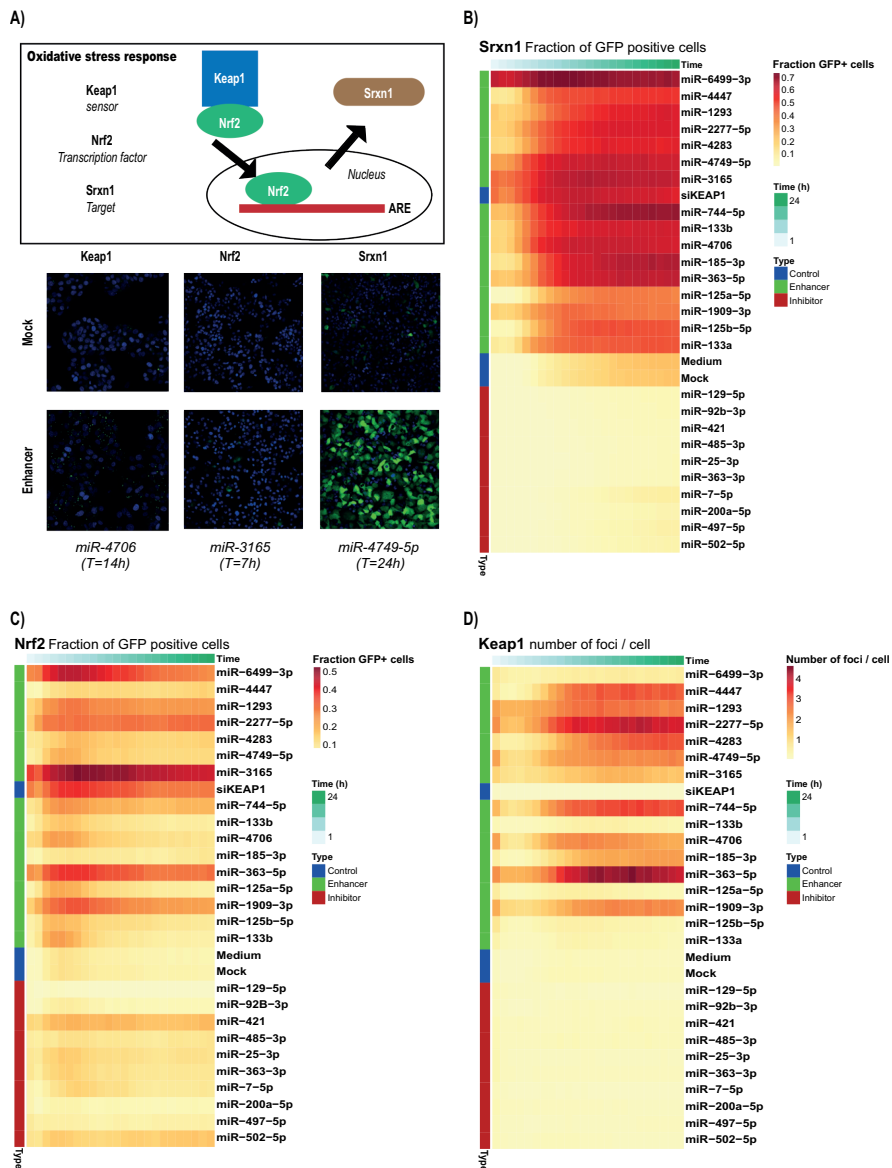


**Figure 3. Effect of candidate microRNAs on the dynamics of Nrf2 pathway activation by CDDO-Me.**

**A)** Schematic overview of the Nrf2 pathway and the corresponding microscope images (mock condition and examples of Sr xn1-enhancing microRNAs **B)** Heatmap showing the fraction of Sr xn1-GFP positive cells after transfection (72 h) of the different selected Sr xn1-enhancing and Sr xn1-inhibiting microRNAs over a 24 h timespan after exposure to 30 nM CDDO-Me. **C)** Heatmap showing the fraction of Nrf2-GFP positive cells after transfection (72 h) of the different selected Sr xn1-enhancing and Sr xn1-inhibiting microRNAs over a 24 h timespan after exposure to 30 nM CDDO-Me. **D)** Heatmap showing the number of Keap1 foci after transfection (72 h) of the different selected Sr xn1-enhancing and Sr xn1-inhibiting microRNAs over a 24 h timespan after exposure to 30 nM CDDO-Me. Values in all heatmaps are mean values from three different experiments.

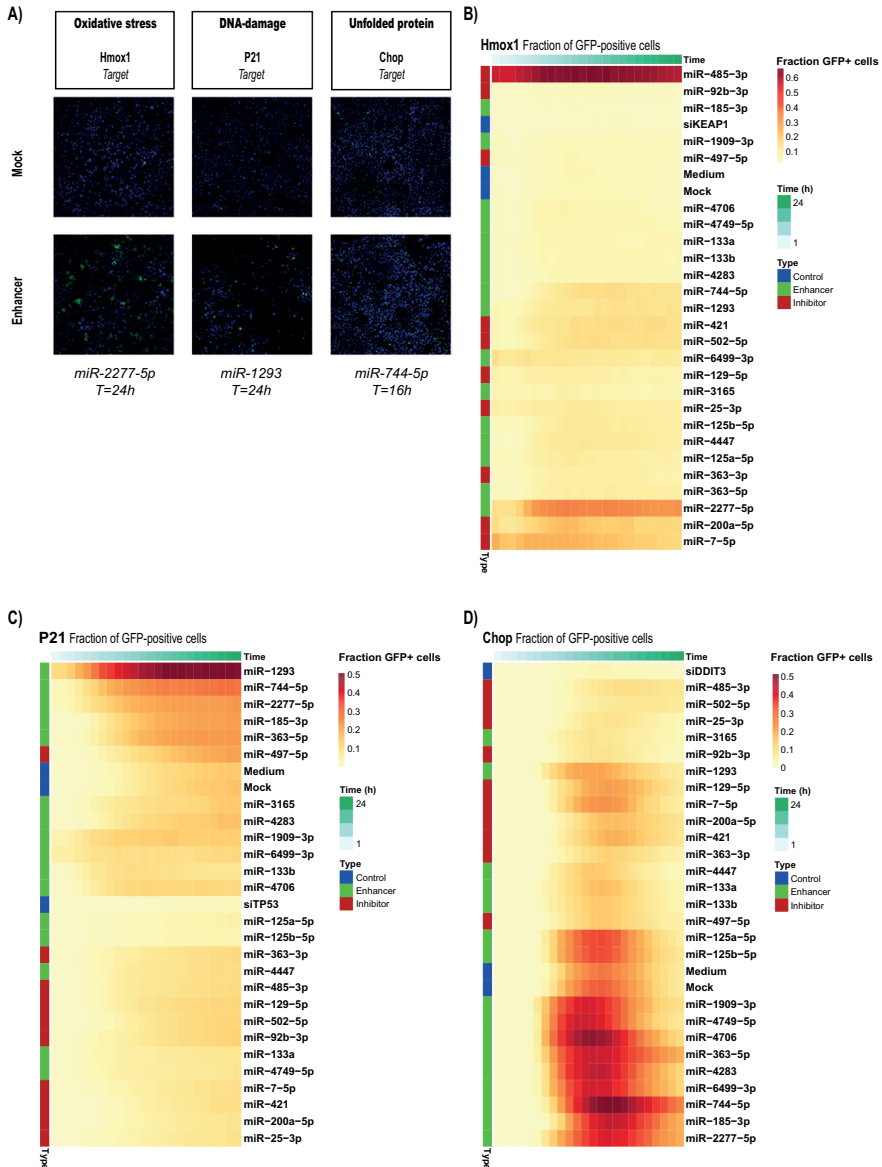


**Figure 4. Effect of candidate microRNAs on cellular stress response pathway activation.**

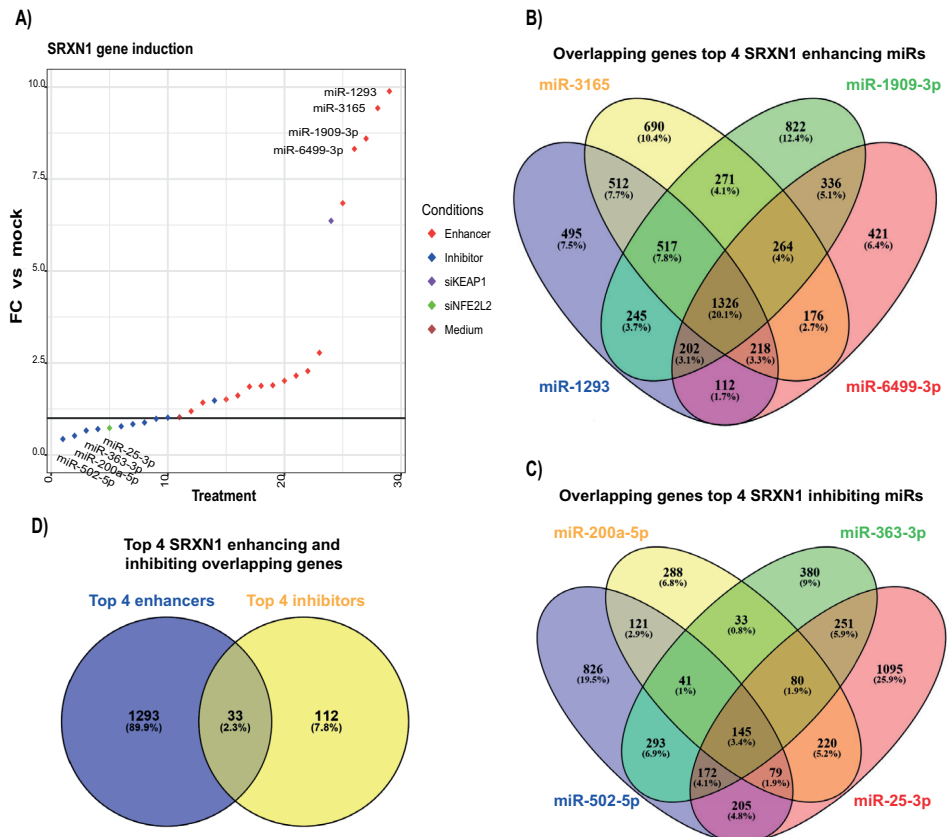
**A)** Microscope images of HepG2 Hmx1-GFP, p21-GFP and Chop-GFP cells (mock condition and examples of *Srxn1* enhancing microRNAs **B)** Heatmap showing the fraction of Hmx1-GFP positive cells after transfection (72 h) of the different selected *Srxn1*-enhancing and *Srxn1* inhibiting microRNAs over a 24 h timespan after 30 nM CDDO-Me exposure. **C)** Heatmap showing the fraction of p21-GFP positive cells after transfection (72 h) of the different selected *Srxn1* enhancing and *Srxn1* inhibiting microRNAs over a 24 h timespan after exposure to 25 μM etoposide. **D)** Heatmap showing the number of Chop-GFP positive cells after transfection (72 h) of the different selected *Srxn1* enhancing and *Srxn1* inhibiting microRNAs over a 24 h timespan after exposure to 6 μM tunicamycin. Values in all heatmaps are mean values from three different experiments.

likely not impact on DNA damage response signaling or modulation of the cell cycle. Yet, we found that in particular some of the Nrf2 pathway enhancing microRNAs did also enhance the induction of p21-GFP reporter activity caused by etoposide, with a remarkable effect by miR-1293. Also some Nrf2 pathway suppressing microRNAs did enhance the etoposide response, including miR-497-5p (Figure 4C). In previous studies we observed that *Srxn1*-GFP activation by drugs that have a liability for drug-induced liver injury is associated with the activation of the unfolded protein response that is represented by the upregulation of the unfolded protein response marker CHOP/DDIT3 (Wink et al. 2018). While siCHOP/DDIT3 abolished the Chop-GFP induction by tunicamycin, microRNAs that caused enhancement of Nrf2 pathway activation did not affect the dynamics of the induction of Chop-GFP. Moreover, none of the microRNAs did affect Chop-GFP levels by itself (Figure 4D).

### Nrf2 pathway modulating microRNA mimic transcriptomic responses of KEAP1 depletion

As a next step we aimed to get more insight on the overall regulation of gene expression profiles of our candidate microRNAs. Therefore we established transcriptome analysis using whole genome targeted RNAseq analysis based on the TempO-Seq approach (Yeakley et al. 2017). We established the transcriptome for all candidate enhancers and suppressors as well as siNFE2L2 (Nrf2) and siKEAP1 as controls, in the absence of any treatment (Figure 5). We observed the suppression and enhancement of basal *Srxn1* expression by the respective candidate microRNAs, with several microRNAs being as potent enhancers as siKEAP1 (i.e. miR-1293, miR-3165, miR-1909-3p and miR-6499-3p), and a panel of repressors as potent as siNFE2L2 (i.e. miR-502-5p, miR-200a-5p, miR-363-3p and miR-25-3p) (Figure 5A). Overall, we did not observe major changes in the expression of the critical Nrf2 pathway components *KEAP1* and *NFE2L2* (see Suppl. Figure 4). We anticipated that the microRNAs that showed similar effects on *Srxn1* expression would have similar gene expression modulation. Therefore, we compared the transcriptome of the top 4 enhancing microRNAs and the top 4 inhibiting microRNAs, based on their ability to induce or repress *SRXN1* and compared their significantly ( $\text{padj} \leq 0.05$ ) differentially expressed (DE) genes (Fig. 5B and C). The top 4 enhancing microRNAs had 20.1 % (1326) DE genes in common, whereas the top 4 inhibiting microRNAs had only 3.4 % DE genes in common. 33 DE expressed genes were found in both the top 4 enhancing and the top 4 inhibiting microRNAs (Figure 5D; Suppl. Table 1). Next, we assessed whether the enhancing and inhibiting miRNAs shared similar pathway modulation as siKEAP1 or siNFE2L2, respectively. We used pathway analysis software to define the top 20 (10 up and 10 down) differentially expressed canonical pathways after siKEAP1 transfection and directly compared these with all the 16 candidate enhancing microRNAs. The effect of most microRNAs were highly comparable

to siKEAP1, with miR-6499-3p being most similar. Importantly, as expected, all candidate enhancing microRNAs showed an upregulation of the Nrf2 signaling pathway. Moreover, also most microRNAs did affect Rho-GTPase signaling pathways comparable to *KEAP1* depletion. Strikingly, various microRNAs did activate the LXR/RXR pathway, which was downregulated by siKEAP1, demonstrating differential regulation (Figure 5E). The suppressing microRNAs showed similar overall Nrf2 signaling pathway suppression as siNFE2L2, except for miR-25-3p. While, miR-363-3p showed most comparable pathway modulation for down regulated pathway, it did not affect the pathways that were strongest upregulated after Nrf2 depletion (Figure 5F). Some pathways were differentially affected by Nrf2 pathway suppressors and enhancers (marked in bold) although not in opposite directions, suggesting to be due to experimental conditions, e.g. transfection reagents. Particularly, the LXR/RXR pathway was strongly activated, possibly due to transactivation by transfection lipids.



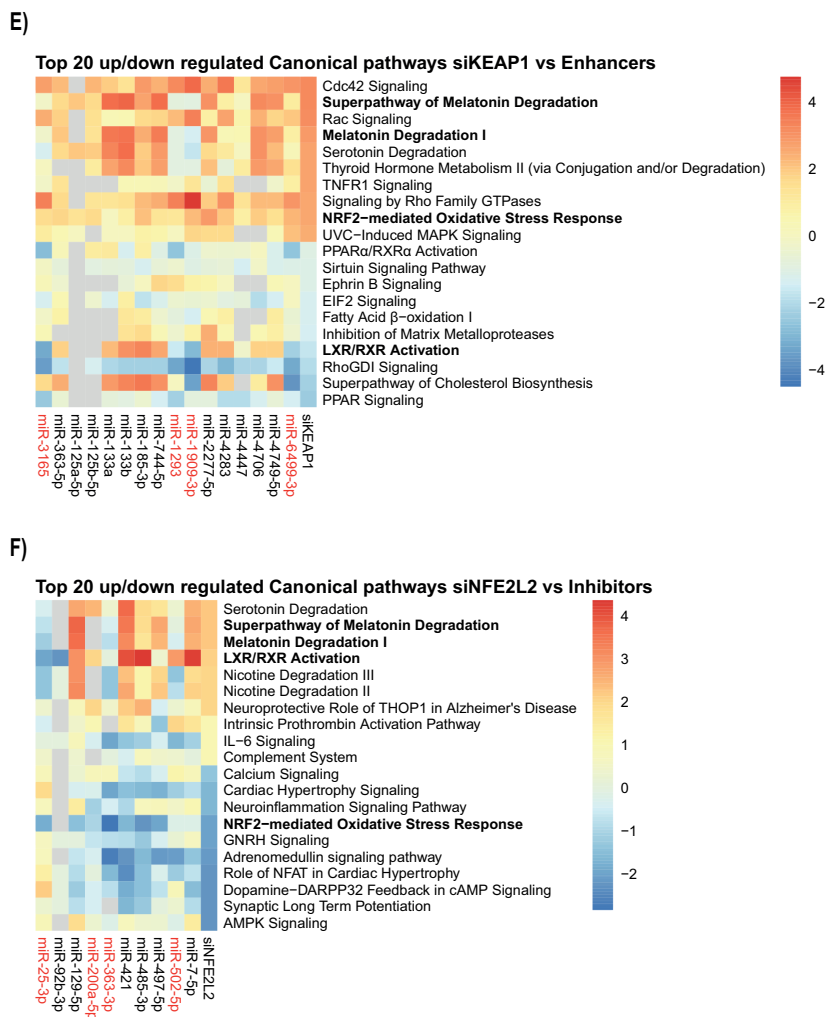
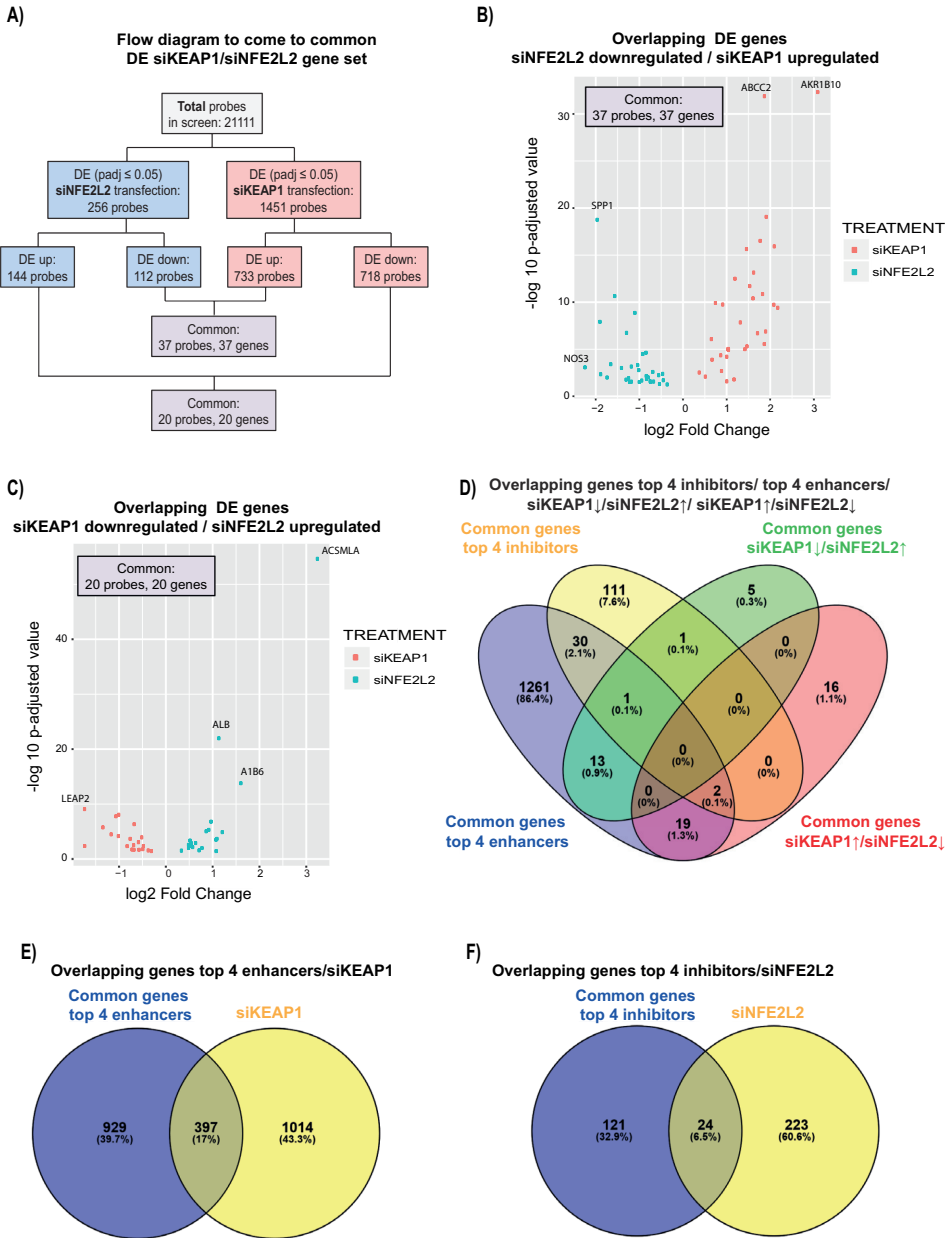


**Figure 5. Effect of candidate Nrf2 pathway modulating miRNA on gene expression.**

**A)** Ranked distribution of the selected microRNAs (enhancer, inhibitor), siKEAP1, siNFE2L2 and medium control for SRXN1 gene induction in HepG2 cells 72 hour after microRNA transfection. **B)** Venn diagram showing the overlapping genes of the top 4 Srxn1 enhancing microRNAs. Percentages are calculated from the total gene-set. **C)** Venn diagram showing the overlapping genes of the top 4 Srxn1 inhibiting microRNAs. Percentages are calculated from the total gene-set. **D)** Venn diagram showing the amount of overlapping DE genes between the overlapping top 4 Srxn1 enhancing and top 4 Srxn1 inhibiting genes. **E)** Heatmap showing clustering of the top 10 upregulated pathways and top 10 downregulated pathways after siKEAP1 transfection compared with the 16 selected enhancing microRNAs. Top 4 is shown in red. **F)** Heatmap showing clustering of the top 10 upregulated pathways and top 10 downregulated pathways after siNFE2L2 transfection compared with the 10 selected inhibiting microRNAs. Gene samples for this measurement were taken after 72 h transfection. Pathway analysis was performed using IPA software. Top 4 is shown in red.

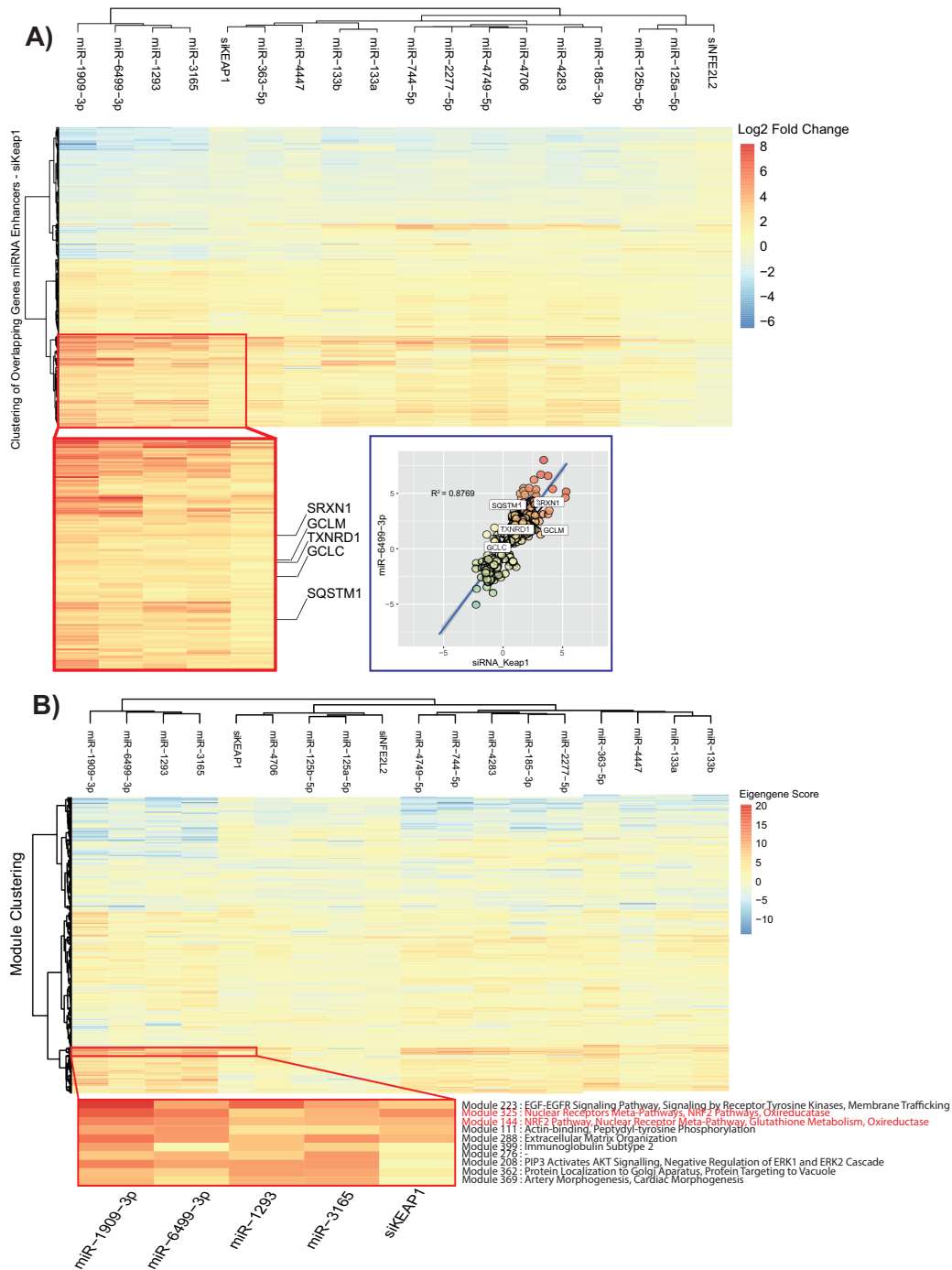
To further assess the impact of the candidate microRNAs on the Nrf2 transcriptional network, we used the siNFE2L2 and siKEAP1 treatments to define the gene set that is under direct control of KEAP1/Nrf2 regulation (Figure 6A). We included genes that were upregulated after *KEAP1* depletion and downregulated after Nrf2 depletion (Figure 6B and Suppl. Table 2), or downregulated by depletion of *KEAP1* and upregulated after depletion of Nrf2 (Figure 6C and Suppl. Table 3). Next, we defined the common denominators of these gene sets and the common genes from the top microRNA candidates. Due to the stringent filtering procedure no genes were observed in overlap for all four groups. *KEAP1* depletion caused the most prominent gene expression changes in concordance with Nrf2 depletion (Figure 6D), therefore we further focused on the genes associated with *KEAP1* depletion and looked for overlap with candidate microRNAs. The genes involved in this group included *bona fide* Nrf2 target genes including *GCLM* and *NQO1*. *SRXN1* and *SQSTM1* were not part of this group, likely because the basic levels are low and are not significantly affected by Nrf2 depletion. We further looked at overlapping genes between the common genes of the top 4 enhancer microRNAs and siKEAP1 (Figure 6E) as well as the overlapping genes between the common genes of the top 4 inhibitors and the siNFE2L2 DE genes (Figure 6F). Enhancer microRNAs showed 397 genes in overlap with siKEAP1 and inhibitor microRNAs showed 24 genes in overlap with siNFE2L2 (see Suppl. Table 4 and 5). *GPF15*, *TRO*, *FRMD4B*, *SPP1*, and *LEAP2* were found in both sets. Together, these respective 397 and 24 overlapping genes represent various well-established Nrf2 target genes, including *NQO1*, *GCLM* and *GCLC*, thus further supporting the direct modulation of the Nrf2 program by the candidate microRNAs.

To get further quantitative information on gene network activation by the candidate microRNAs we made advantage of co-regulated gene network analysis using our previously established toxicogenomic map tool ([https://txg-mapr.eu/WGCNA\\_PHH/TGGATEs\\_PHH/](https://txg-mapr.eu/WGCNA_PHH/TGGATEs_PHH/)) (Callegaro et al. 2021; Langfelder and Horvath 2008; Sutherland et al. 2018). Here we focused on the 397 genes (478 probes) that were in overlap between the top 4 *Srxn1* enhancing microRNAs (miR-1909-3p, miR-6499-3p, miR-1293, and miR-3165) and siKEAP1 (Figure 6E and Suppl. Table 4) for which similar patterns in gene expression were observed (Figure 7A; Suppl. Figure 5). The fold change expression data for these genes was used to calculate the gene network module activation score, eigengene score (EGS), of each module (Figure 7B). A cluster of modules was strongly enhanced by these microRNAs and siKEAP1 representing two oxidative stress gene network modules: Module 144 and Module 325. Module 144 contained *SRXN1* as well as other Nrf2 target genes including *TXRDN1* and *GCLM* and was strongly activated by all four enhancing microRNAs and siKEAP1 (Figure 7C). The pattern of expression of genes within both Module 144 and Module 325 was similar for these microRNAs and siKEAP1 (Figure 7C and Suppl. Figure 6).



**Figure 6. Overview of Nrf2 pathway specific overlapping genes.**

**A)** Flow diagram used to create the two gene sets used in figure B,C, and D. **B)** Overlapping DE genes downregulated after siNFE2L2 transfection and upregulated after siKEAP1 transfection. **C)** Overlapping DE genes downregulated with siKEAP1 transfection and upregulated with siNFE2L2 transfection. **D)** Venn diagram showing the overlap between four gene sets: common genes top 4 inhibitors, common genes top 4 enhancers, siKEAP1 upregulated and siNFE2L2 downregulated genes, and siKEAP1 downregulated and siNFE2L2 upregulated genes. **E)** Overlapping genes top 4 enhancers with DE genes after siKEAP1 transfection. **F)** Overlapping genes top 4 inhibitors with DE genes after siNFE2L2 transfection.



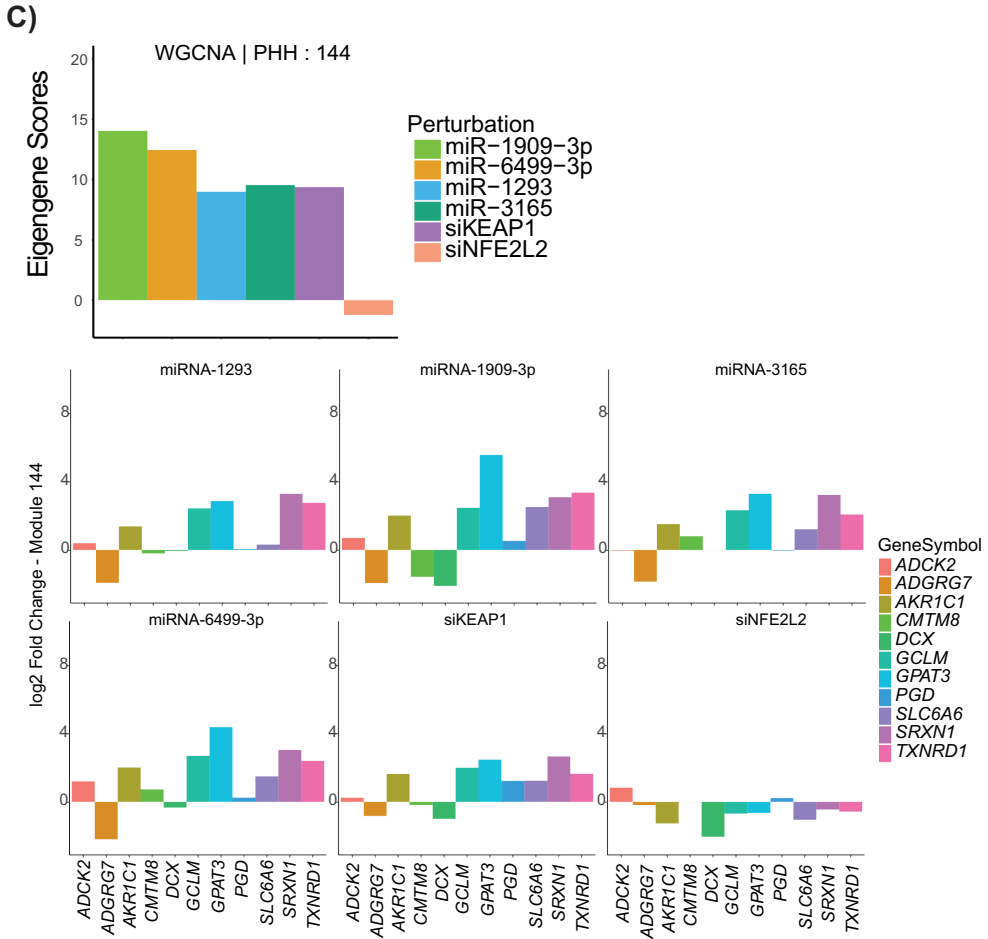


**Figure 7. Profiling overlapped genes between microRNA enhancers and siKEAP1.**

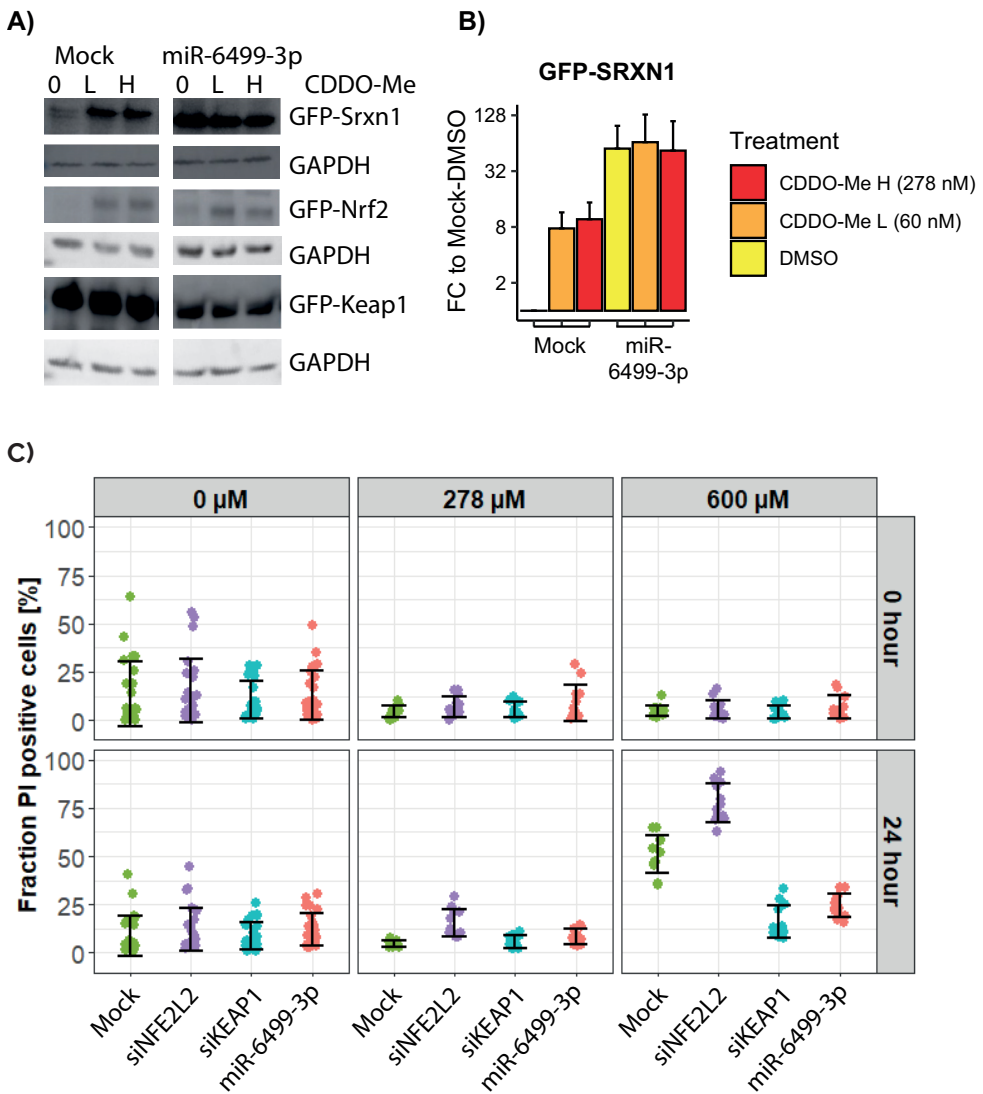
**A)** A heatmap showing log<sub>2</sub> fold change values of overlapped genes between microRNA (miRNA) enhancers and siKEAP1. Hierarchical clustering of the miRNAs, siKEAP1 and siNFE2L2 shows a cluster of 4 strongest miRNA enhancers (miR-1909-3p, miR-6499-3p, miR-1293, and miR-3165) identical to the miRNAs exhibiting strong capacity of inducing SRXN1. An enriched area (red box) is identified in the responses of these strong miRNA and siKEAP1 showing high log<sub>2</sub> fold change > 2 of oxidative stress related genes. Correlation analysis exhibit high Pearson correlation value (0.87) between the strongest miRNA enhancer, miR-6499-3p with siKEAP1. **B)** Pathway enrichment analysis of overlapped genes utilizing TXG-MAPr-PHH showing strong activation of oxidative stress pathways (Module 144 and Module 325) among the other 8 highest activated pathways upon the perturbation of miRNA enhancers. A correlation plot of miR-6499-3p and siKEAP1 at the module (gene network) level shows poor correlation (0.32) with more prominent responses upon miR-6499-3p perturbation. **C)** The eigengene score of Module 144 and the log<sub>2</sub> fold change values of its gene memberships in 4 miRNA enhancers, siKEAP1, and siNFE2L2.

### miR-6499-3p affects KEAP1 expression and susceptibility to oxidative stress-induced cell death

Finally, we aimed at understanding the mechanism of Nrf2 pathway modulation of candidate microRNAs. Given that the seed region of a microRNA is important for target recognition (Bartel 2009), as a further validation of our microRNA screen we anticipated that our candidate microRNAs would share the seed region and would therefore have a similar mode-of-action on Nrf2 pathway modulation. We looked at a seed region of 7 nucleotides (Bartel 2009; Mullany et al. 2016). Intriguingly, we found that three of the ten inhibiting microRNAs had the same seed region sequence (miR-25-3p, miR-363-3p, miR-92b-3p; AUUGCAC). Also two of the sixteen selected enhancing microRNAs have the same seed region sequence (miR-4749-5p, miR-4706; GCGGGGA). For miR-25-3p, miR-363-3p and miR-92b-3p we observed considerable overlap in the differential expressed genes (Suppl. Figure 8A). 85 % of the genes differently expressed with miR-4706 overlap with the genes differently expressed by miR-4749-5p, which is 33% of the total genes differentially expressed by miR-4749-5p. This might indicate a similar mode-of-action of the seed region and did involve the Nrf2 pathway modulation (Suppl. Figure 8B). We also anticipated that our candidate microRNAs would directly target Nrf2 pathway components. Therefore we specifically evaluated the effect of our candidate microRNAs on *NFE2L2* and *KEAP1* as well as *SRXN1* using microRNA target prediction tools from IPA, MiRDB, and Targetscan. Only one suppressing microRNA, miR-129-5p, was predicted to target Nrf2, suggesting a direct inhibition of Srxn1 activation due to lack of Nrf2. Three of the enhancing microRNAs, miR-6499-3p, miR-505-5p and miR-4283, were predicted to target *KEAP1*. Counter intuitively all three *KEAP1* targeting microRNAs were also predicted to target *SRXN1*, yet did not block Srxn1-GFP induction. Other *SRXN1* targeting microRNA predictions involved miR-185-3p and miR-200a-5p, an enhancing and suppressing microRNA, respectively. None of the other candidate microRNAs were predicted to target *KEAP1*, *Nrf2/NFE2L2* or *SRXN1*.

We selected miR-6499-3p for some final validation studies since miR-6499-3p showed strong downregulation of Keap1-GFP in conjunction with strong induction of Nrf2 levels and Srxn1-GFP induction (Fig. 2). Moreover, miR-6499-3p correlated highly with siKEAP1 at the transcriptional level. Expression of miR-6499-3p in the reporter cell lines also strongly reduced the expression of GFP-Keap1 at protein level which was consistent with upregulation of Srxn1 and Nrf2 to a maximal level such that further induction by CDDO-Me was not detected (Fig. 8A and B). Given this maximal induction of the Nrf2 response, we then wondered whether miR-6499-3p could be protective for oxidative stress-induced cell death. For this purpose we exposed wild type HepG2 cells to nitrofurantoin (NTF) that causes formation of oxidative stress in hepatocytes that leads to cell death (Wijaya et al. 2021). While siNFE2L2 treatment

highly sensitized cells to NTF treatment, miR-6499-3p was protective against NTF-induced cell death in a similar manner as siKEAP1 treatment. This indicates that the activation of the Nrf2 pathway by miR-6499-3p provides a powerful cytoprotection.



D)

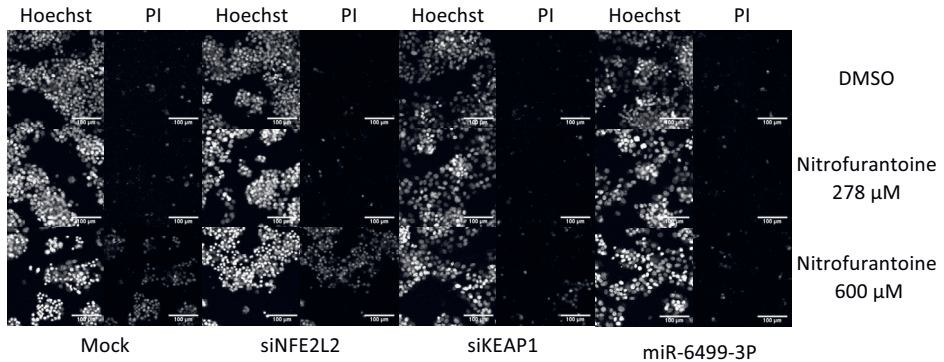


**Figure 8. Effect of miR-6499-3p on cytoprotection.**

Respective GFP-Keap1, GFP-Nrf2 and GFP-Srxn1 HepG2 reporter cell lines with mock or miR-6499-3p transfection were treated with two different concentrations of CDDO-Me followed by Western blotting for GFP-Srxn1, GFP-Nrf2 and GFP-Keap1 **(A)** and quantification of the bands from three independent Western blots **(B)**. **(C)** Wild type HepG2 transfected with miR-6499-3p, siNFE2L2 or siKEAP1 were treated with nitrofurantoin followed by high content imaging of onset of cell death based on propidium iodide (PI) staining. Fraction of PI positive cells after exposure to 0, 278 or 600  $\mu\text{M}$  nitrofurantoin is shown for the different treatments. Data are derived from 3 independent experiments. For each treatment x concentration x transfection combination, 1 well was imaged at 4 different positions. Error bars indicate the standard deviation around the mean. The viability is expressed in cell fraction PI positive. **(D)** Microscopic images of wild type HepG2 cells stained with Hoechst 33342 and PI after transfection with miR-6499-3p and exposure to nitrofurantoin. Scale bar is equivalent to 100  $\mu\text{m}$ .

## DISCUSSION

Here we applied a systematic microRNA mimic screen to uncover the microRNA landscape that modulates Nrf2 activation. For this purpose we used an established Srxn1-GFP BAC reporter HepG2 cell line that is under full control by Nrf2, in combination with live cell confocal microscopy to evaluate Nrf2 activity in individual cells at the population level. We used CDDO-Me (bardoxolone methyl) as activator of the Nrf2-mediated Srxn1-GFP expression and discerned microRNAs that either inhibit or enhance the induction of Srxn1-GFP by CDDO-Me. We successfully uncovered ten microRNAs that inhibit and sixteen microRNAs that enhance Nrf2 pathway activation. Transcriptome analysis identified that these microRNAs mimicked the activity of either siNFE2L2 or siKEAP1. miR-6499-3p was validated by microRNA target prediction as a candidate microRNA that targets *KEAP1*, and closely mimicked the effect of *KEAP1* knockdown at the transcriptional level as well as cytoprotective level.

Our microRNA mimic screen has identified various microRNAs that can modulate the expression of the Nrf2 target *Srxn1*. Although the effect of this set of twenty-six microRNAs on *Srxn1* expression was in various cases highly comparable with the effect of siKEAP1 and siNFE2L2, there was no consistent modulation of Nrf2 and Keap1 expression based on the Nrf2-GFP and Keap1-GFP reporters (see Figure 3). Thus, miR-6499-3p showed clear correlation between strong *Srxn1*-GFP induction and increased levels of Nrf2-GFP and reduced levels of Keap1-GFP, in concordance with targeting *KEAP1* by this microRNA (Figure 3 and 8). A similar pattern was observed for miR-3165. Yet, in contrast, while miR-4749-5p showed a similar strong induction of *Srxn1*-GFP and a transcriptome modulation similar to miR-6499-3p and siKEAP1, the regulation of Nrf2-GFP was not affected, suggesting other mechanism of enhanced *Srxn1*-GFP expression independent from Nrf2 modulation. Importantly, miR-6499-3p closely mimicked the effect of siKEAP1 at various levels including protection against a high concentration of nitrofurantoin, a drug that can cause oxidative stress-induced cell death in hepatocytes (Wijaya et al. 2021).

We used CDDO-Me (bardoxolone-methyl) in our screen to identify Nrf2-modulating microRNAs. CDDO-Me is a known, potent, inducer of the Nrf2 pathway. CDDO-Me is able to activate the Nrf2 pathway by direct binding to Cys151 of Keap1 and therefore inhibiting Keap1 function (Cleasby et al. 2014). Moreover, CDDO-Me was used in different clinical trials for modulation of the antioxidant response (Wang et al. 2014). We systematically validated that our candidate microRNAs also impacted on the *Srxn1*-GFP induction by other potent pro-oxidants, DEM and tBHQ, that also modulate *Srxn1*-GFP levels through Nrf2 activation (Bischoff et al. 2019). This indicates that our candidate microRNAs are genuine modulators of the Nrf2 pathway and may have implications in diverse pro-oxidant conditions.

We could clearly classify candidate Nrf2 pathway modulating microRNAs into two groups, those that either enhance or inhibit the *Srxn1* response. *Hmox1* has been a classical oxidative stress marker for various tissues. We observed no induction of *Hmox1* reporter activity by CDDO-Me or siKEAP1. Also the microRNAs that enhanced the *Srxn1*-GFP response did themselves not impact on *HMOX1* gene expression, while *GCLM* gene expression was clearly enhanced by enhancer microRNAs. Some other microRNAs did impact on *Hmox1*-GFP activity, but this could not be related back to specific patterns of either Nrf2-GFP, Keap1-GFP and *Srxn1*-GFP modulation. Similarly, while some candidate microRNAs did affect either the unfolded protein response pathway or the DNA damage response pathway, with Chop-GFP and p21-GFP as respective biomarkers, these effects were not directly associated with potency of *Srxn1*-GFP reporter activity. These observations indicate that i) overexpression of these microRNAs does not lead to an overt general cellular perturbation creating a

state of overwhelming “general” cellular stress, consequently leading to apoptosis and/or cell death, and ii) the delicate balance of how different microRNAs can modulate one or multiple stress response signaling pathways.

Activation of the Nrf2 pathway is divided into two mechanisms: canonical and non-canonical (Silva-Islas and Maldonado 2018). The canonical pathway is defined by the Keap1/Nrf2/ARE axes activated by electrophilic compounds and ROS. The non-canonical pathway involves the activation of the Nrf2 pathway by proteins also capable of disrupting the Keap1-Nrf2 interaction. Using three different prediction tools we determined how our candidate microRNAs would target the canonical Nrf2 pathway components. We found miR-4283 to directly target *Srxn1*. Surprisingly, we found miR-4283 to enhance *Srxn1*. miR-129-5p, was predicted to target Nrf2, suggesting a direct inhibition of *Srxn1* activation due to lack of Nrf2. Three of the enhancing miRNAs, miR-6499-3p, miR-505-5p and miR-4283, were predicted to target *KEAP1*. Loss of Keap1-GFP levels was indeed observed in the Keap1-GFP reporter cell line, confirming the target prediction. Previous studies have reported individual Nrf2 pathway modulating microRNAs, including miR-122, miR-144, miR-155, miR-196, miR34a/b/c and miR-200a (reviewed in (Cheng et al. 2013)). In our study only miR-200a-5p was found to suppress *Srxn1* activity. However in other studies, miR-200a is described to target *KEAP1*, leading to Nrf2 induction (Sun et al. 2016; Zhao et al. 2018) which was not observed in our hands. miR-7 activates *HMOX1* and *GCLM*, two downstream targets of the Nrf2 pathway, by direct targeting *KEAP1* in the human neuroblastoma cell SH-SY5Y (Kabaria et al. 2015). In our study, we found miR-7-5p to suppress *GCLM*, but to induce HO-1 on protein level. These different observations are possibly due to cell type differences.

We have identified both positive and negative microRNA regulators of the Nrf2 pathway. Since we did not observe overt cytotoxic responses of these candidate microRNA, we anticipate that such microRNAs that target the Nrf2 pathway could be used for therapeutic approaches. *KEAP1* mutations in cancer are critical drivers in cancer progression as well as drug resistance, in particular in lung cancer (Cuadrado et al. 2019). Such mutations lead to constitutive Nrf2 activation, hence, microRNA that would inhibit the Nrf2 pathway could possibly impact on cancer progression. Similarly, various pathophysiology situations, such as ischemic reperfusion injury of tissues that highly depend on oxidative phosphorylation and involve severe oxidative stress, could benefit from Nrf2 pathway activation (Cuadrado et al. 2019); microRNAs that activate the Nrf2 pathway, such as miR-6499-3p, could be promising therapeutic modulators to protect cells from detrimental oxidative stress cell injury. This would require systematic studies on the efficacy and safety of such microRNA therapeutic approaches.

In conclusion, our study for the first time elucidate the spectrum of microRNAs that target the Nrf2 signaling pathway. The Nrf2 pathway is of critical importance in cancer development and progression, with various *KEAP1* and Nrf2 mutations that act as cancer drivers, as well as in various degenerative disease settings. Therefore, we anticipate that our selected enhancing and inhibiting microRNA might be interesting as putative biomarkers and/or microRNA therapeutics to generically modulate the Nrf2 pathway.

## ACKNOWLEDGEMENTS

This work was supported by the Ministry of Defence of the Netherlands and the European Commission Horizon2020 EU-ToxRisk project (grant nr 681002).

## REFERENCES

- Agarwal V, Bell GW, Nam JW, Bartel DP (2015) Predicting effective microRNA target sites in mammalian mRNAs. *Elife* 4 doi:10.7554/eLife.05005
- Almeida MI, Reis RM, Calin GA (2011) MicroRNA history: discovery, recent applications, and next frontiers. *Mutat Res* 717(1-2):1-8 doi:10.1016/j.mrfmmm.2011.03.009
- Baird L, Yamamoto M (2020) The Molecular Mechanisms Regulating the KEAP1-NRF2 Pathway. *Molecular and Cellular Biology* 40(13):e00099-20 doi:10.1128/MCB.00099-20
- Balasubramanian S, Gunasekaran K, Sasidharan S, Jeyamanickavel Mathan V, Perumal E (2020) MicroRNAs and Xenobiotic Toxicity: An Overview. *Toxicol Rep* 7:583-595 doi:10.1016/j.toxrep.2020.04.010
- Bartel DP (2009) MicroRNAs: target recognition and regulatory functions. *Cell* 136(2):215-33 doi:10.1016/j.cell.2009.01.002
- Bartoszewska S, Kochan K, Madanecki P, et al. (2013) Regulation of the unfolded protein response by microRNAs. *Cell Mol Biol Lett* 18(4):555-578 doi:10.2478/s11658-013-0106-z
- Bischoff LJM, Kuijper IA, Schimming JP, et al. (2019) A systematic analysis of Nrf2 pathway activation dynamics during repeated xenobiotic exposure. *Arch Toxicol* 93(2):435-451 doi:10.1007/s00204-018-2353-2
- Borchert GM, Lanier W, Davidson BL (2006) RNA polymerase III transcribes human microRNAs. *Nat Struct Mol Biol* 13(12):1097-101 doi:10.1038/nsmb1167
- Brennecke J, Stark A, Russell RB, Cohen SM (2005) Principles of microRNA-target recognition. *PLoS Biol* 3(3):e85 doi:10.1371/journal.pbio.0030085
- Callegaro G, Kunnen SJ, Trairatphisan P, et al. (2021) The human hepatocyte TXG-MAPr: WGCNA transcriptomic modules to support mechanism-based risk assessment. *bioRxiv:2021.05.17.444463* doi:10.1101/2021.05.17.444463
- Cheng X, Ku CH, Siow RC (2013) Regulation of the Nrf2 antioxidant pathway by microRNAs: New players in micromanaging redox homeostasis. *Free Radic Biol Med* 64:4-11 doi:10.1016/j.freeradbiomed.2013.07.025
- Cleasby A, Yon J, Day PJ, et al. (2014) Structure of the BTB domain of Keap1 and its interaction with the triterpenoid antagonist CDDO. *PLoS One* 9(6):e98896 doi:10.1371/journal.pone.0098896
- Cople IM, den Hollander W, Callegaro G, et al. (2019) Characterisation of the NRF2 transcriptional network and its response to chemical insult in primary human hepatocytes: implications for prediction of drug-induced liver injury. *Arch Toxicol* 93(2):385-399 doi:10.1007/s00204-018-2354-1
- Cuadrado A, Manda G, Hassan A, et al. (2018) Transcription Factor NRF2 as a Therapeutic Target for Chronic Diseases: A Systems Medicine Approach. *Pharmacol Rev* 70(2):348-383 doi:10.1124/pr.117.014753
- Cuadrado A, Rojo AI, Wells G, et al. (2019) Therapeutic targeting of the NRF2 and KEAP1 partnership in chronic diseases. *Nature reviews Drug discovery* 18(4):295-317 doi:10.1038/s41573-018-0008-x
- Djuranovic S, Nahvi A, Green R (2012) miRNA-Mediated Gene Silencing by Translational Repression Followed by mRNA Deadenylation and Decay. *Science* 336(6078):237 doi:10.1126/science.1215691
- Dodson M, de la Vega MR, Cholanians AB, Schmidlin CJ, Chapman E, Zhang DD (2019) Modulating NRF2 in Disease: Timing Is Everything. *Annu Rev Pharmacol Toxicol* 59:555-575 doi:10.1146/annurev-pharmtox-010818-021856

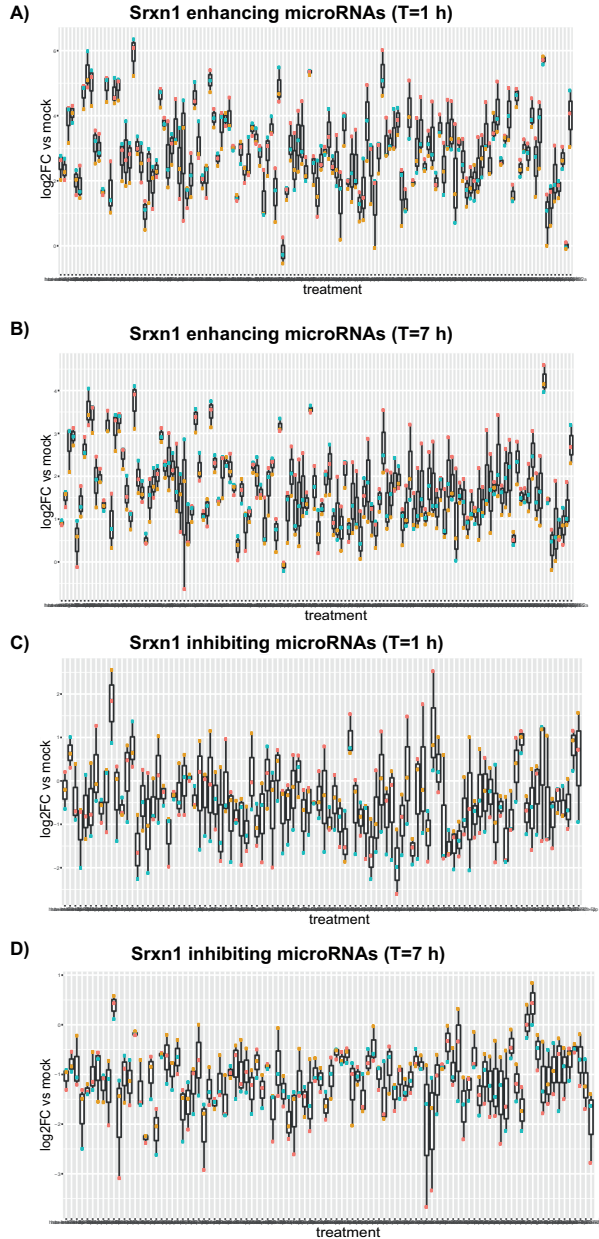
- Filipowicz W, Bhattacharyya SN, Sonenberg N (2008) Mechanisms of post-transcriptional regulation by microRNAs: are the answers in sight? *Nature Reviews Genetics* 9(2):102-114 doi:10.1038/nrg2290
- Hayes JD, McMahon M, Chowdhry S, Dinkova-Kostova AT (2010) Cancer Chemoprevention Mechanisms Mediated Through the Keap1–Nrf2 Pathway. *Antioxidants & Redox Signaling* 13(11):1713-1748 doi:10.1089/ars.2010.3221
- Herpers B, Wink S, Fredriksson L, et al. (2016) Activation of the Nrf2 response by intrinsic hepatotoxic drugs correlates with suppression of NF-kappaB activation and sensitizes toward TNFalpha-induced cytotoxicity. *Arch Toxicol* 90(5):1163-79 doi:10.1007/s00204-015-1536-3
- Hiemstra S, Ramaiahgari SC, Wink S, et al. (2019) High-throughput confocal imaging of differentiated 3D liver-like spheroid cellular stress response reporters for identification of drug-induced liver injury liability. *Archives of Toxicology* 93(10):2895-2911 doi:10.1007/s00204-019-02552-0
- Hou L, Wang D, Baccarelli A (2011) Environmental chemicals and microRNAs. *Mutat Res* 714(1-2):105-12 doi:10.1016/j.mrfmmm.2011.05.004
- Itoh K, Wakabayashi N, Katoh Y, et al. (1999) Keap1 represses nuclear activation of antioxidant responsive elements by Nrf2 through binding to the amino-terminal Neh2 domain. *Genes & Development* 13(1):76-86 doi:10.1101/gad.13.1.76
- Kabaria S, Choi DC, Chaudhuri AD, Jain MR, Li H, Junn E (2015) MicroRNA-7 activates Nrf2 pathway by targeting Keap1 expression. *Free Radic Biol Med* 89:548-56 doi:10.1016/j.freeradbiomed.2015.09.010
- Keum YS, Choi BY (2014) Molecular and chemical regulation of the Keap1-Nrf2 signaling pathway. *Molecules* 19(7):10074-89 doi:10.3390/molecules190710074
- Kobayashi A, Kang MI, Okawa H, et al. (2004) Oxidative stress sensor Keap1 functions as an adaptor for Cul3-based E3 ligase to regulate proteasomal degradation of Nrf2. *Mol Cell Biol* 24(16):7130-9 doi:10.1128/MCB.24.16.7130-7139.2004
- Lam JK, Chow MY, Zhang Y, Leung SW (2015) siRNA Versus miRNA as Therapeutics for Gene Silencing. *Mol Ther Nucleic Acids* 4:e252 doi:10.1038/mtna.2015.23
- Langfelder P, Horvath S (2008) WGCNA: an R package for weighted correlation network analysis. *BMC Bioinformatics* 9(1):559 doi:10.1186/1471-2105-9-559
- Lee RC, Feinbaum RL, Ambros V (1993) The *C. elegans* heterochronic gene *lin-4* encodes small RNAs with antisense complementarity to *lin-14*. *Cell* 75(5):843-54 doi:10.1016/0092-8674(93)90529-y
- Lee Y, Kim M, Han J, et al. (2004) MicroRNA genes are transcribed by RNA polymerase II. *EMBO J* 23(20):4051-60 doi:10.1038/sj.emboj.7600385
- Lewis BP, Shih IH, Jones-Rhoades MW, Bartel DP, Burge CB (2003) Prediction of mammalian microRNA targets. *Cell* 115(7):787-98 doi:10.1016/s0092-8674(03)01018-3
- Lin S, Gregory RI (2015) MicroRNA biogenesis pathways in cancer. *Nat Rev Cancer* 15(6):321-33 doi:10.1038/nrc3932
- Love MI, Huber W, Anders S (2014) Moderated estimation of fold change and dispersion for RNA-seq data with DESeq2. *Genome Biol* 15(12):550-550 doi:10.1186/s13059-014-0550-8
- McMahon M, Thomas N, Itoh K, Yamamoto M, Hayes JD (2006) Dimerization of substrate adaptors can facilitate cullin-mediated ubiquitylation of proteins by a “tethering” mechanism: a two-site interaction model for the Nrf2-Keap1 complex. *J Biol Chem* 281(34):24756-68 doi:10.1074/jbc.M601119200
- Medina MV, Sapochnik D, Garcia Sola M, Coso O (2020) Regulation of the Expression of Heme Oxygenase-1: Signal Transduction, Gene Promoter Activation, and Beyond. *Antioxid Redox Signal* 32(14):1033-1044 doi:10.1089/ars.2019.7991

- Mendell JT, Olson EN (2012) MicroRNAs in stress signaling and human disease. *Cell* 148(6):1172-87 doi:10.1016/j.cell.2012.02.005
- Mullany LE, Herrick JS, Wolff RK, Slattery ML (2016) MicroRNA Seed Region Length Impact on Target Messenger RNA Expression and Survival in Colorectal Cancer. *PLoS One* 11(4):e0154177 doi:10.1371/journal.pone.0154177
- Peter ME (2010) Targeting of mRNAs by multiple miRNAs: the next step. *Oncogene* 29(15):2161-2164 doi:10.1038/onc.2010.59
- Poser I, Sarov M, Hutchins JR, et al. (2008) BAC TransgeneOmics: a high-throughput method for exploration of protein function in mammals. *Nat Methods* 5(5):409-15 doi:10.1038/nmeth.1199
- Riffo-Campos AL, Riquelme I, Brebi-Mieville P (2016) Tools for Sequence-Based miRNA Target Prediction: What to Choose? *Int J Mol Sci* 17(12) doi:10.3390/ijms17121987
- Sangokoya C, Doss JF, Chi JT (2013) Iron-responsive miR-485-3p regulates cellular iron homeostasis by targeting ferroportin. *PLoS Genet* 9(4):e1003408 doi:10.1371/journal.pgen.1003408
- Schimming JP, Ter Braak B, Niemeijer M, Wink S, van de Water B (2019) System Microscopy of Stress Response Pathways in Cholestasis Research. *Methods in molecular biology* (Clifton, NJ) 1981:187-202 doi:10.1007/978-1-4939-9420-5\_13
- Silva-Islas CA, Maldonado PD (2018) Canonical and non-canonical mechanisms of Nrf2 activation. *Pharmacol Res* 134:92-99 doi:10.1016/j.phrs.2018.06.013
- Starega-Roslan J, Krol J, Koscianska E, et al. (2010) Structural basis of microRNA length variety. *Nucleic Acids Research* 39(1):257-268 doi:10.1093/nar/gkq727
- Sun X, Zuo H, Liu C, Yang Y (2016) Overexpression of miR-200a protects cardiomyocytes against hypoxia-induced apoptosis by modulating the kelch-like ECH-associated protein 1-nuclear factor erythroid 2-related factor 2 signaling axis. *Int J Mol Med* 38(4):1303-11 doi:10.3892/ijmm.2016.2719
- Sutherland JJ, Webster YW, Willy JA, et al. (2018) Toxicogenomic module associations with pathogenesis: a network-based approach to understanding drug toxicity. *The Pharmacogenomics Journal* 18(3):377-390 doi:10.1038/tpj.2017.17
- Wang YY, Yang YX, Zhe H, He ZX, Zhou SF (2014) Bardoxolone methyl (CDDO-Me) as a therapeutic agent: an update on its pharmacokinetic and pharmacodynamic properties. *Drug Des Devel Ther* 8:2075-88 doi:10.2147/DDDT.S68872
- Wijaya LS, Rau C, Braun TS, et al. (2021) Stimulation of de novo glutathione synthesis by nitrofurantoin for enhanced resilience of hepatocytes. *Cell Biol Toxicol* doi:10.1007/s10565-021-09610-3
- Wink S, Hiemstra S, Herpers B, van de Water B (2017) High-content imaging-based BAC-GFP toxicity pathway reporters to assess chemical adversity liabilities. *Arch Toxicol* 91(3):1367-1383 doi:10.1007/s00204-016-1781-0
- Wink S, Hiemstra SW, Huppelschoten S, Klip JE, van de Water B (2018) Dynamic imaging of adaptive stress response pathway activation for prediction of drug induced liver injury. *Arch Toxicol* 92(5):1797-1814 doi:10.1007/s00204-018-2178-z
- Wong N, Wang X (2015) miRDB: an online resource for microRNA target prediction and functional annotations. *Nucleic Acids Res* 43(Database issue):D146-52 doi:10.1093/nar/gku1104
- Wu S, Huang S, Ding J, et al. (2010) Multiple microRNAs modulate p21Cip1/Waf1 expression by directly targeting its 3' untranslated region. *Oncogene* 29(15):2302-2308 doi:10.1038/onc.2010.34

- Yamamoto M, Kensler TW, Motohashi H (2018) The KEAP1-NRF2 System: a Thiol-Based Sensor-Effector Apparatus for Maintaining Redox Homeostasis. *Physiol Rev* 98(3):1169-1203 doi:10.1152/physrev.00023.2017
- Yeakley JM, Shepard PJ, Goyena DE, VanSteenhouse HC, McComb JD, Seligmann BE (2017) A trichostatin A expression signature identified by TempO-Seq targeted whole transcriptome profiling. *PLoS One* 12(5):e0178302 doi:10.1371/journal.pone.0178302
- Zhang DD, Lo SC, Cross JV, Templeton DJ, Hannink M (2004) Keap1 is a redox-regulated substrate adaptor protein for a Cul3-dependent ubiquitin ligase complex. *Mol Cell Biol* 24(24):10941-53 doi:10.1128/MCB.24.24.10941-10953.2004
- Zhang Y, Gordon GB (2004) A strategy for cancer prevention: Stimulation of the Nrf2-ARE signaling pathway. *Molecular Cancer Therapeutics* 3(7):885
- Zhao XJ, Yu HW, Yang YZ, et al. (2018) Polydatin prevents fructose-induced liver inflammation and lipid deposition through increasing miR-200a to regulate Keap1/Nrf2 pathway. *Redox Biol* 18:124-137 doi:10.1016/j.redox.2018.07.002
- Zipper LM, Mulcahy RT (2002) The Keap1 BTB/POZ dimerization function is required to sequester Nrf2 in cytoplasm. *J Biol Chem* 277(39):36544-52 doi:10.1074/jbc.M206530200

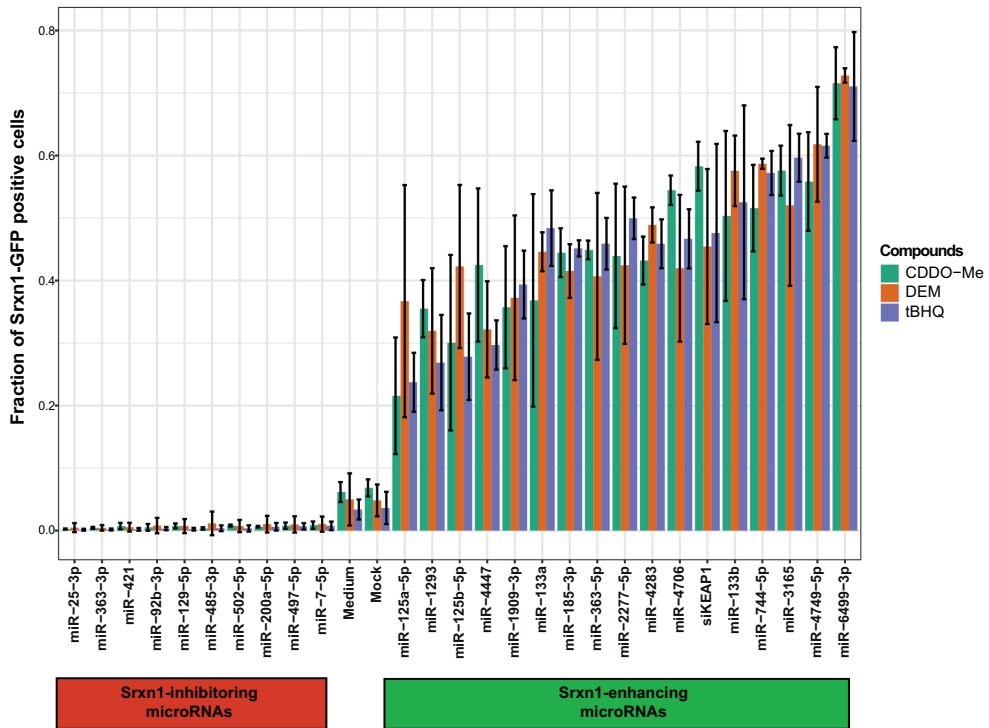
## SUPPLEMENTAL MATERIALS

3



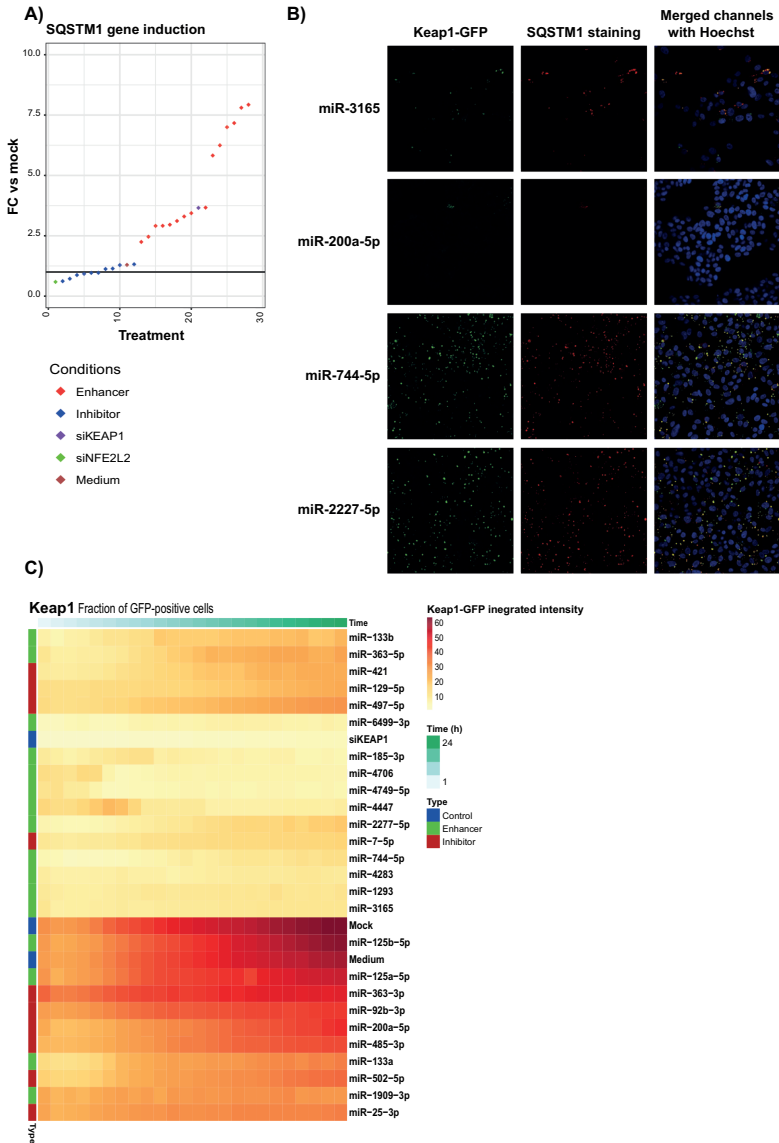
**Supplemental Figure 1. Overview of the distribution of the three measurements of the secondary screen.**

**A)** Srnx1 enhancing microRNAs measured 1 h after 30 nM CDDO-Me exposure. **B)** Srnx1 enhancing microRNAs measured 7 h after 30 nM CDDO-Me exposure. **C)** Srnx1 inhibiting microRNAs measured 1 h after 30 nM CDDO-Me exposure. **D)** Srnx1 inhibiting microRNAs measured 7 h after 30 nM CDDO-Me exposure. Three replicates are shown with different color (red, blue, yellow). Log<sub>2</sub>FC vs mock condition is plotted for the different microRNAs.



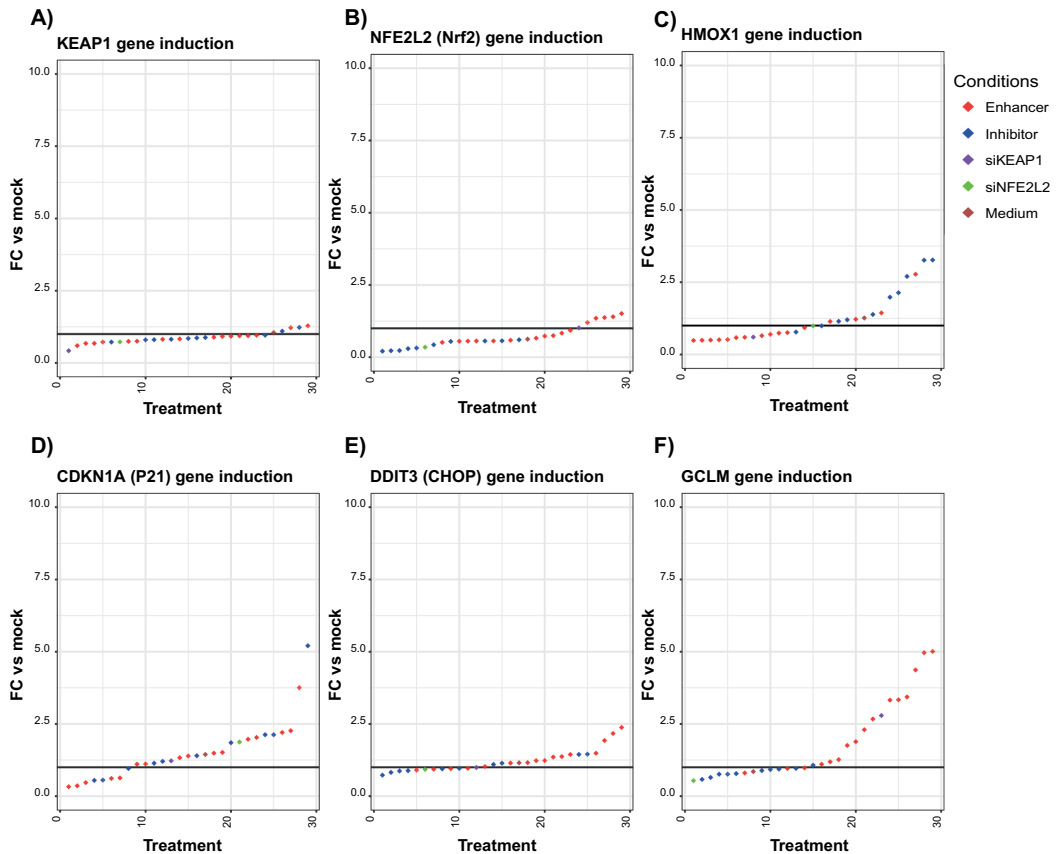
**Supplemental Figure 2. Comparison of the effect of different Nrf2-activating compounds.**

Comparison of the fraction of Srxn1-GFP positive cells after microRNA transfection and exposure to CDDO-Me (30nM), DEM (100 $\mu$ M), or tBHQ (100 $\mu$ M). Error bars represent the SD (n=3).



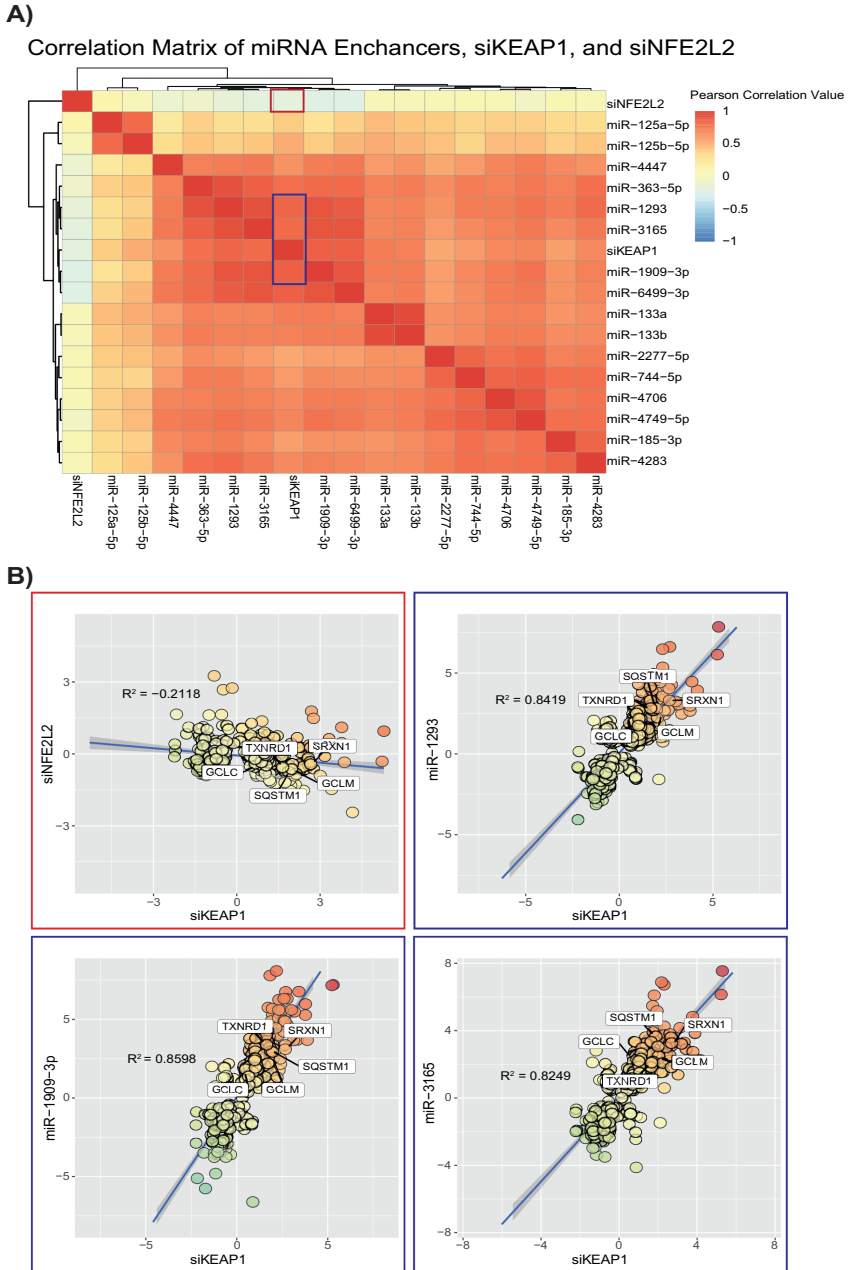
**Supplemental Figure 3. Effect of microRNAs on Keap1-GFP and SQSTM1 mediated autophagosome formation.**

**A)** Ranked distribution of SQSTM1 gene induction (Fold change vs mock). Srxn1 enhancing microRNAs are shown in red, Srxn1 inhibiting microRNAs are shown in blue, siKEAP1 transfection is shown in purple, siNFE2L2 transfection is shown in green, and the medium condition is shown in brown. Values are the mean of three different experiments. The top 4 enhancers are represented in the top 5 SQSTM1 upregulating microRNAs (enhancers) **B)** Microscope images (confocal) after transfection of 4 different microRNAs in HepG2-keap1-GFP cells. Green = Keap1-GFP, red = SQSTM1 staining, Blue = nucleus staining (Hoechst). Pictures are taken 24 h after microRNA transfection and exposure to 30 nM CDDO-Me. **C)** Keap1-GFP-integrated intensity (mean of three different experiments) is shown over time (1-24 h) after microRNA transfection, siKEAP1 transfection, mock, and medium condition after exposure to 30 nM CDDO-Me.



#### Supplemental Figure 4. Expression of different stress pathway related genes.

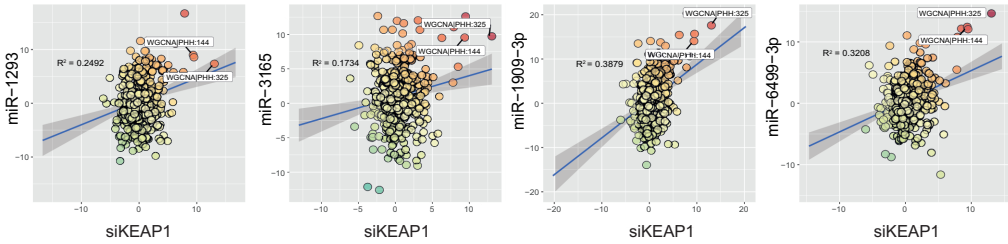
**A)** Ranked distribution of KEAP1 gene induction (Fold change vs mock). miR-6499-3p can be found directly after siKEAP1. **B)** Ranked distribution of NFE2L2 gene induction (Fold change vs mock). **C)** Ranked distribution of HMOX1 gene induction (Fold change vs mock). **D)** Ranked distribution of CDKN1A gene induction (Fold change vs mock). miR-6499-3p is the most CDKN1A suppressing microRNA. miR-25-3p and miR-744 the most CDKN1A enhancing microRNAs. **E)** Ranked distribution of DDIT3 gene induction (Fold change vs mock). **F)** Ranked distribution of GCLM gene induction (Fold change vs mock). Top 4 microRNA enhancers found with GCLM are the top 4 microRNA enhancers found with SRXN1.



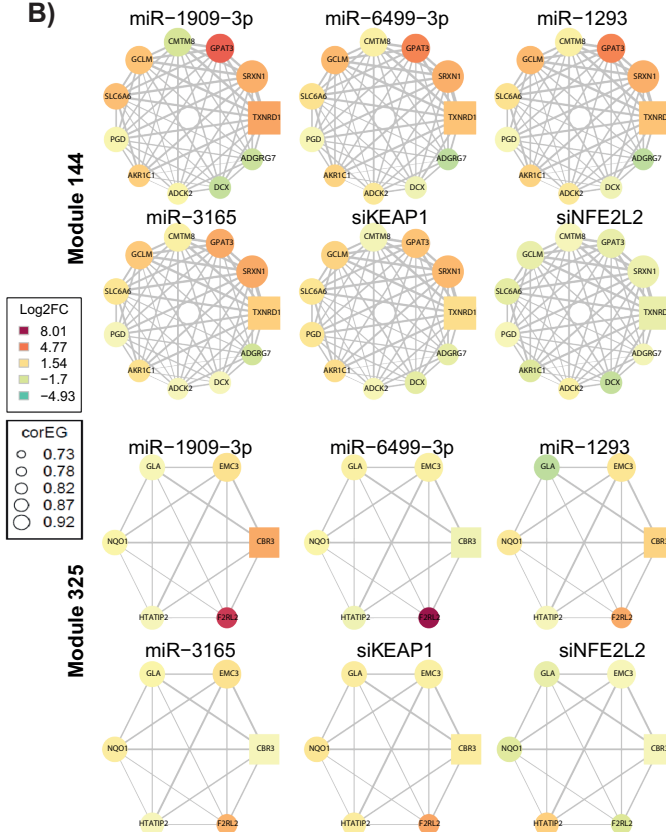
**Supplemental Figure 5. Correlation analysis between siKEAP1, miRNA enhancer, and siNFE2L2 based on the overlapping genes of siKEAP1 with miRNA enhancer.**

**A)** A heatmap illustrating the correlation matrix of miRNA enhancers at the gene levels. An enriched area highlighted in the blue box shows high Pearson correlation values ( $>0.8$ ) between siKEAP1 and 4 strongest microRNA enhancers mentioned in Figure 1A. **B)** Correlation plots between microRNA enhancers and siKEAP1 showing high correlation value ( $>0.8$ ).

A)

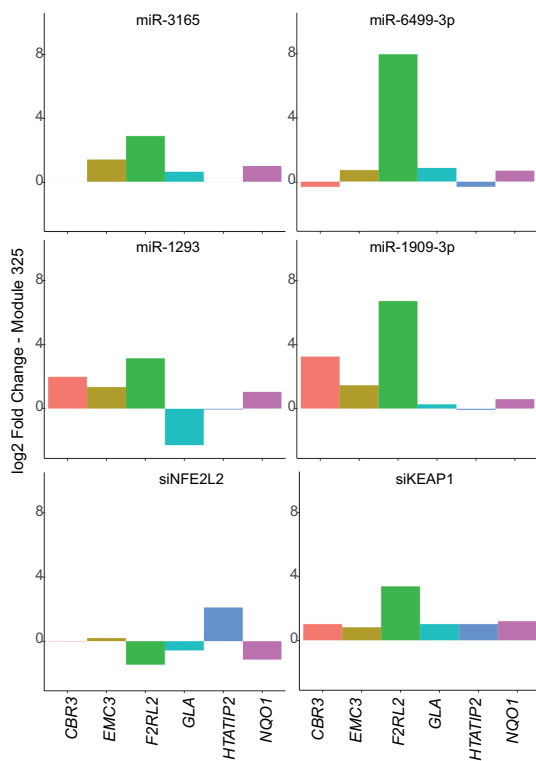
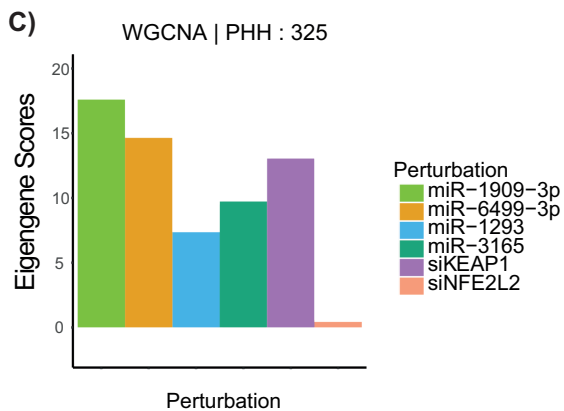


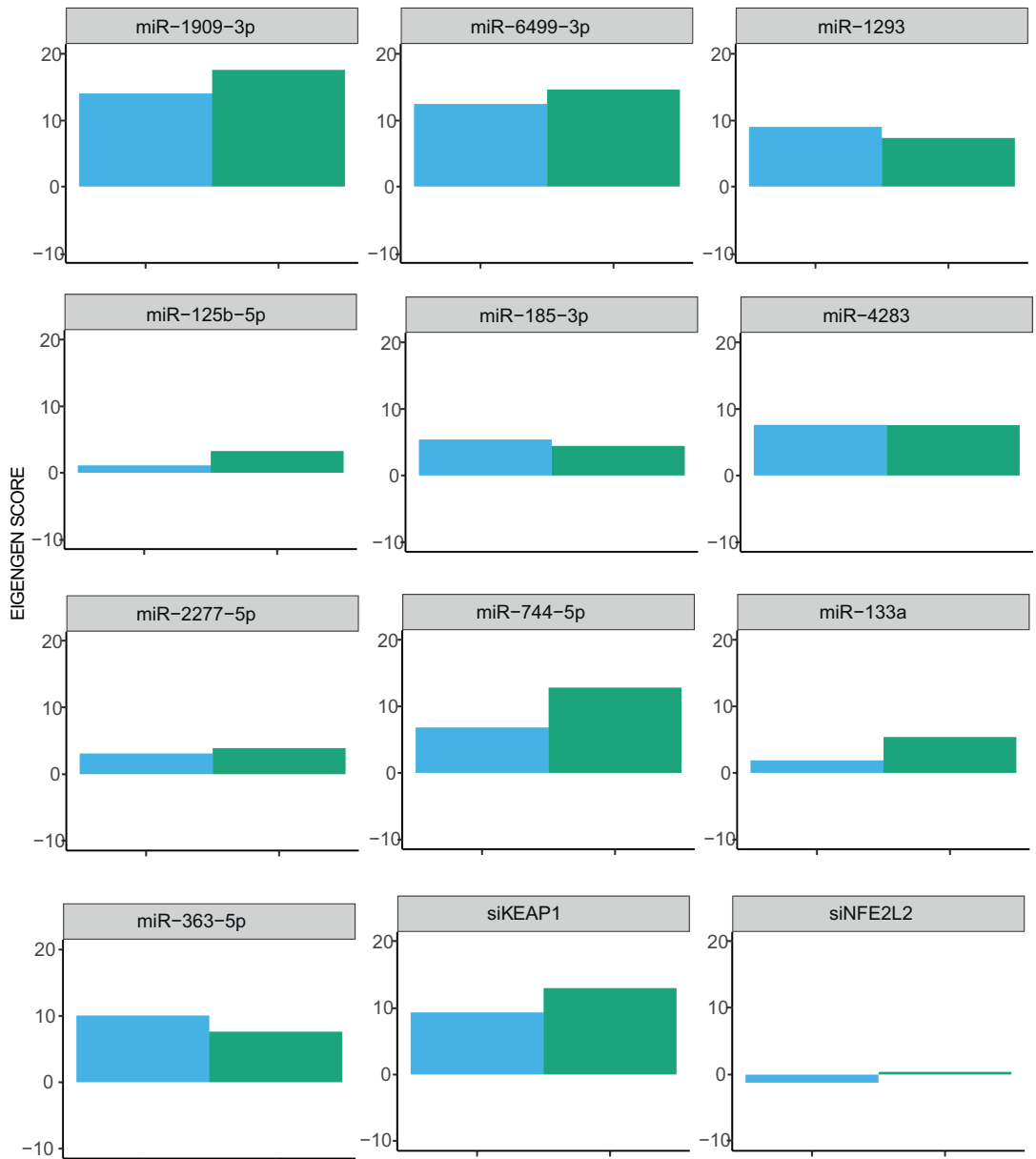
B)



### Supplemental Figure 6. Pathway enrichment analysis utilizing PHH TXG-MAPr platform.

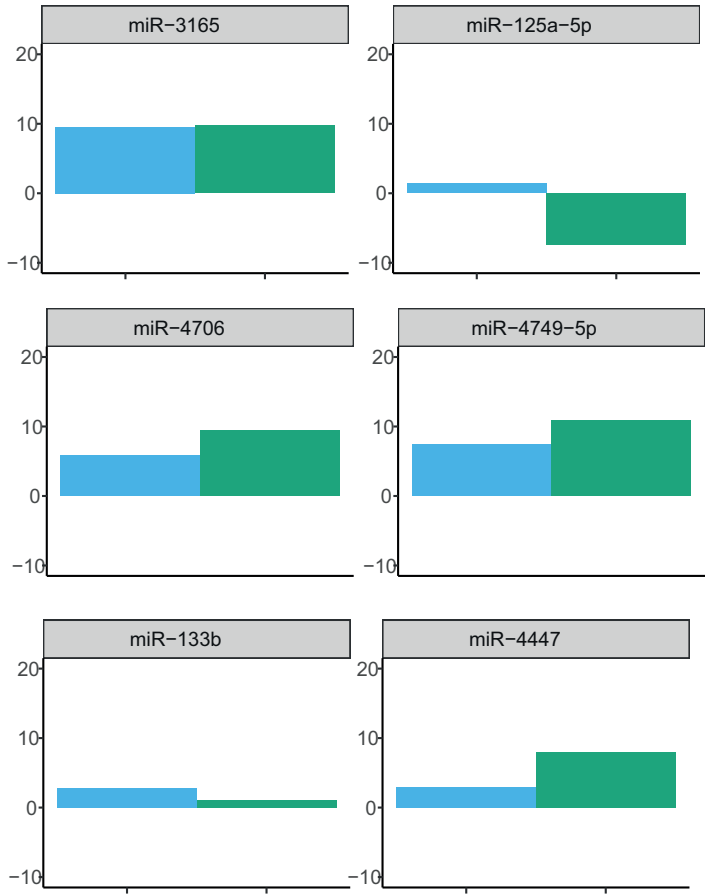
**A)** Correlation plots between microRNA enhancers and siKEAP1 at the module level show poor correlation ( $< 0.4$ ) with broader responses of microRNA activating multiple pathways. **B)** The expression of module membership of Module 144 and Module 325 upon the perturbation of microRNA enhancers, siKEAP1, and siNFE2L2. **C)** The Eigengene score of Module 325 and the log 2 fold change values of its gene memberships in 4 microRNA enhancers, siKEAP1, and siNFE2L2.





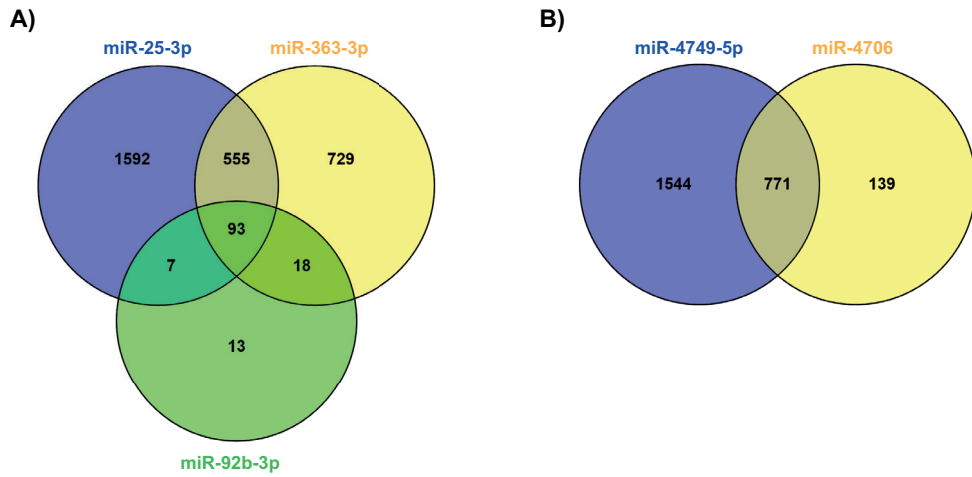
**Supplemental Figure 7. Eigengene scores of Module 144 and Module 325 of microRNA enhancers, siKEAP1 and siNFE2L2.**

The Eigengene score of Module 144 and 325 upon the perturbation of microRNA enhancers (besides the 4 strongest microRNA enhancers), siKEAP1, and siNFE2L2.



siRNA

- WGCNA|PHH:144
- WGCNA|PHH:325



**Supplemental Figure 8. MicroRNAs with the same seed region have overlap in transcriptome modulation.**

**A)** Overlapping genes of the inhibiting microRNAs miR-25-3p, miR-363-3p and miR-92b-3p with seed region AUUGCAC. **B)** Overlapping genes of the enhancing microRNAs miR-4706 and miR-4749-5p with seed region GCGGGGA.

**Supplemental Table 1. 33 Differentially expressed genes overlapping between the top 4 microRNAs that either enhance or inhibit the Srxn1-GFP response.**

Probe_ID	miR-1293			miR-3615			miR-1909-3p		
	padj	log2FC	lfcSE	padj	log2FC	lfcSE	padj	log2FC	lfcSE
ADD3_16935	0.00	-0.55	0.15	0.00	-1.08	0.16	0.00	0.67	0.14
ANXA3_16294	0.00	2.16	0.25	0.00	2.73	0.25	0.00	3.81	0.24
DNAJC18_18335	0.00	1.36	0.20	0.00	1.75	0.20	0.00	1.46	0.20
EMP3_18953	0.00	3.37	0.21	0.00	1.53	0.22	0.00	4.10	0.21
FRMD4B_12533	0.00	2.07	0.21	0.00	2.34	0.21	0.00	2.86	0.20
GBP3_16959	0.00	3.55	0.38	0.00	3.75	0.38	0.00	5.09	0.37
GDF15_18329	0.00	3.22	0.27	0.00	4.23	0.27	0.00	1.21	0.27
GDF15_2621	0.00	2.26	0.24	0.00	2.99	0.24	0.00	0.96	0.24
GEMIN5_22827	0.00	-1.29	0.18	0.00	-1.32	0.18	0.00	-1.33	0.18
GOT1_2737	0.00	-0.62	0.17	0.00	0.93	0.16	0.00	1.13	0.16
IER3_3214	0.00	0.94	0.28	0.00	1.97	0.28	0.00	2.14	0.28
IQCJ-SCHIP1_13265	0.00	2.59	0.31	0.00	1.87	0.32	0.00	3.58	0.30
LEAP2_26340				0.01	-3.92	1.35	0.01	-4.00	1.35
LEAP2_28319	0.00	-2.04	0.30	0.00	-2.12	0.30	0.00	-3.12	0.33
LMO7_27443	0.01	0.65	0.20	0.00	1.61	0.20	0.00	1.08	0.20
MCM3_4072	0.00	-1.79	0.16	0.00	-1.67	0.16	0.00	-1.97	0.16
MGST2_15529	0.00	-1.72	0.31	0.00	-2.02	0.31	0.00	-1.88	0.31
MGST2_27509	0.00	-0.63	0.18				0.00	-1.81	0.20
MGST2_27508							0.01	-1.14	0.36
MIXL1_15283	0.00	-1.64	0.31	0.00	-1.69	0.31	0.00	-2.84	0.31
NBPF14_33921	0.00	1.59	0.22	0.00	1.38	0.22	0.00	1.63	0.22
NSMF_14995	0.00	-1.87	0.45	0.00	-2.03	0.46	0.01	-1.35	0.45
NSMF_4729	0.00	-1.40	0.18	0.00	-1.52	0.18	0.03	-0.46	0.17
NT5C3A_11648	0.00	-0.98	0.18	0.01	-0.53	0.18	0.00	-0.96	0.18
NTN4_11596	0.01	1.51	0.46	0.00	2.67	0.43	0.00	2.42	0.43
RAB5B_22829	0.00	1.06	0.14	0.00	0.84	0.14	0.04	0.35	0.14
SCN9A_17603	0.00	1.56	0.35	0.00	2.42	0.34	0.00	2.20	0.34
SLC25A10_6388				0.03	-2.97	1.13			
SLC25A10_21880	0.00	-1.94	0.21	0.00	-1.92	0.21	0.00	-2.13	0.21
SLC40A1_20629	0.00	1.02	0.15	0.00	2.07	0.15	0.00	1.31	0.15
SLC6A14_6512	0.00	-1.72	0.23	0.00	-0.93	0.23	0.00	-1.71	0.23
SPP1_6720	0.00	-0.97	0.24	0.04	0.60	0.24	0.01	0.72	0.24
TEP1_18252	0.00	2.12	0.22	0.00	2.64	0.22	0.00	1.79	0.22

Probe_ID	miR-1293			miR-3615			miR-1909-3p		
	padj	log2FC	lfcSE	padj	log2FC	lfcSE	padj	log2FC	lfcSE
TMEM214_24547	0.00	-0.96	0.16	0.00	-1.12	0.16	0.00	-1.24	0.16
TRIM28_20524	0.00	-0.65	0.12	0.00	-1.01	0.12	0.00	-1.12	0.12
TRO_28012	0.03	2.50	0.95	0.00	3.43	0.93			
TRO_26673	0.01	2.39	0.80	0.00	3.00	0.79	0.01	2.57	0.80
TRO_7352	0.00	1.90	0.32	0.00	2.00	0.32	0.00	1.64	0.32
UBXN7_22634	0.00	1.66	0.25	0.00	1.42	0.26	0.00	1.67	0.25
VPS13C_24266	0.00	1.52	0.20	0.00	1.28	0.21	0.02	0.61	0.21
ZMYND19_11392	0.00	-0.85	0.16	0.00	-0.78	0.16	0.00	-0.59	0.16

Probe_ID	miR-6499-3p			miR-502-5p			miR-200a-5p		
	padj	log2FC	lfcSE	padj	log2FC	lfcSE	padj	log2FC	lfcSE
ADD3_16935	0.00	1.35	0.14	0.00	-0.66	0.18	0.00	1.50	0.14
ANXA3_16294	0.01	0.85	0.25	0.00	1.22	0.29	0.01	-1.09	0.30
DNAJC18_18335	0.00	0.98	0.20	0.00	1.01	0.23	0.00	0.94	0.20
EMP3_18953	0.00	1.98	0.22	0.01	0.81	0.25	0.02	-0.80	0.25
FRMD4B_12533	0.00	1.94	0.21	0.00	1.37	0.24	0.00	1.12	0.23
GBP3_16959	0.00	4.21	0.37	0.00	2.56	0.43	0.01	1.51	0.41
GDF15_18329	0.00	3.56	0.27				0.00	-1.19	0.27
GDF15_2621	0.00	2.93	0.24	0.03	-0.83	0.29	0.00	-1.49	0.27
GEMIN5_22827	0.00	-0.94	0.18	0.00	-1.03	0.20	0.00	-0.97	0.18
GOT1_2737	0.00	1.00	0.16	0.00	-0.85	0.20	0.01	-0.60	0.17
IER3_3214	0.00	2.18	0.28	0.00	-1.48	0.34	0.00	-1.90	0.31
IQCJ-SCHIP1_13265	0.00	2.82	0.30	0.00	2.23	0.34	0.00	1.86	0.33
LEAP2_26340	0.01	-4.26	1.35						
LEAP2_28319	0.00	-2.73	0.31	0.00	1.44	0.31	0.00	1.38	0.27
LMO7_27443	0.02	0.57	0.20	0.00	1.12	0.23	0.02	0.66	0.20
MCM3_4072	0.00	-2.11	0.16	0.00	-1.11	0.19	0.04	-0.47	0.16
MGST2_15529	0.02	-0.85	0.30	0.03	0.97	0.34			
MGST2_27509	0.01	-0.55	0.18				0.00	-0.71	0.19
MGST2_27508							0.03	-1.13	0.37
MIXL1_15283	0.00	-1.27	0.31	0.00	-1.29	0.36	0.00	-1.38	0.31
NBPF14_33921	0.00	1.21	0.22	0.00	1.13	0.25	0.03	0.70	0.23
NSMF_14995	0.05	-1.13	0.45						
NSMF_4729				0.00	-0.75	0.20	0.00	-1.46	0.18
NT5C3A_11648	0.01	-0.59	0.18	0.01	-0.68	0.21	0.01	-0.65	0.18

Probe_ID	miR-6499-3p			miR-502-5p			miR-200a-5p		
	padj	log2FC	lfcSE	padj	log2FC	lfcSE	padj	log2FC	lfcSE
NTN4_11596	0.00	1.87	0.44	0.00	2.36	0.48	0.00	1.97	0.45
RAB5B_22829	0.00	0.98	0.14	0.02	0.48	0.16	0.00	1.11	0.14
SCN9A_17603	0.00	1.97	0.34	0.00	2.72	0.38	0.04	1.07	0.37
SLC25A10_6388									
SLC25A10_21880	0.00	-1.44	0.21	0.00	-1.16	0.24	0.00	-0.79	0.21
SLC40A1_20629	0.00	3.09	0.15	0.00	1.51	0.18	0.00	1.32	0.15
SLC6A14_6512	0.00	-1.26	0.23	0.00	-1.15	0.26	0.00	-1.75	0.23
SPP1_6720	0.00	1.46	0.24	0.00	1.01	0.28	0.00	-0.99	0.24
TEP1_18252	0.00	1.61	0.22	0.03	0.72	0.26	0.00	-0.97	0.26
TMEM214_24547	0.01	-0.47	0.15	0.00	-0.95	0.18	0.00	-0.68	0.15
TRIM28_20524	0.00	-1.21	0.12	0.00	-0.67	0.14	0.00	-0.46	0.12
TRO_28012				0.00	3.16	0.88			
TRO_26673				0.05	2.81	1.05			
TRO_7352	0.00	1.24	0.33	0.00	2.05	0.35	0.03	1.02	0.34
UBXN7_22634	0.00	1.25	0.26	0.00	1.31	0.29	0.01	0.94	0.27
VPS13C_24266	0.00	0.99	0.21	0.00	1.43	0.23	0.00	0.89	0.21
ZMYND19_11392	0.00	-0.61	0.16	0.00	-0.78	0.18	0.00	-0.69	0.16

Probe_ID	miR-363-3p			miR-25-3p		
	padj	log2FC	lfcSE	padj	log2FC	lfcSE
ADD3_16935	0.00	1.01	0.14	0.00	0.90	0.14
ANXA3_16294	0.00	1.65	0.25	0.00	1.56	0.25
DNAJC18_18335	0.00	1.18	0.20	0.00	1.40	0.20
EMP3_18953	0.00	2.42	0.21	0.00	1.84	0.22
FRMD4B_12533	0.01	0.77	0.22	0.03	0.67	0.23
GBP3_16959	0.00	2.12	0.39	0.00	2.48	0.39
GDF15_18329				0.00	-1.02	0.27
GDF15_2621	0.00	-0.98	0.25	0.00	-1.39	0.26
GEMIN5_22827	0.00	-0.84	0.18	0.00	-0.69	0.18
GOT1_2737	0.00	-0.82	0.17	0.01	-0.60	0.17
IER3_3214	0.00	-1.64	0.30	0.00	-2.09	0.31
IQCJ-SCHIP1_13265	0.00	2.44	0.31	0.00	2.35	0.31
LEAP2_26340						
LEAP2_28319	0.00	-1.46	0.28	0.00	-1.78	0.29

Probe_ID	miR-363-3p			miR-25-3p		
	padj	log2FC	lfcSE	padj	log2FC	lfcSE
LMO7_27443	0.04	0.58	0.20	0.00	0.77	0.20
MCM3_4072	0.01	-0.57	0.16	0.02	-0.48	0.16
MGST2_15529	0.04	-0.86	0.30			
MGST2_27509				0.00	-0.88	0.19
MGST2_27508				0.02	-1.10	0.36
MIXL1_15283	0.00	-2.66	0.31	0.00	-2.13	0.31
NBPF14_33921	0.00	0.90	0.22	0.00	1.30	0.22
NSMF_14995	0.01	-1.52	0.45			
NSMF_4729	0.00	-1.05	0.17	0.00	-1.72	0.18
NT5C3A_11648	0.02	-0.58	0.18	0.00	-1.26	0.18
NTN4_11596	0.01	1.50	0.44	0.00	2.10	0.44
RAB5B_22829	0.01	0.46	0.14	0.00	0.91	0.14
SCN9A_17603	0.01	1.22	0.35	0.03	1.02	0.36
SLC25A10_6388				0.03	2.16	0.78
SLC25A10_21880	0.00	-1.22	0.21	0.00	-1.19	0.21
SLC40A1_20629	0.00	1.70	0.15	0.00	1.76	0.15
SLC6A14_6512	0.00	-3.15	0.24	0.00	-3.56	0.24
SPP1_6720	0.00	-1.50	0.24	0.00	-1.44	0.24
TEP1_18252	0.00	0.87	0.22	0.00	0.85	0.23
TMEM214_24547	0.00	-0.71	0.15	0.00	-1.05	0.16
TRIM28_20524	0.01	-0.41	0.12	0.00	-0.42	0.12
TRO_28012				0.02	2.79	0.95
TRO_26673	0.04	2.30	0.80	0.01	2.72	0.80
TRO_7352	0.00	1.41	0.32	0.00	1.87	0.32
UBXN7_22634	0.02	0.82	0.26	0.02	0.80	0.27
VPS13C_24266	0.00	1.06	0.20	0.00	0.78	0.21
ZMYND19_11392	0.00	-0.63	0.16	0.00	-0.85	0.16

**Supplemental Table 2. Common 37 genes of siKEAP1 upregulated genes/ siNFE2L2 downregulated genes and effects of Nrf2 pathway enhancing and inhibiting microRNAs.**

Probe_ID	siKEAP1			siNFE2L2		
	padj	log2FC	lfcSE	padj	log2FC	lfcSE
ABCC2_26620	1.1E-32	1.9E+00	1.5E-01	4.4E-02	-5.1E-01	1.6E-01
ACTG1_85	2.6E-03	4.0E-01	1.0E-01	4.9E-02	-3.4E-01	1.0E-01
AKR1B10_19908	4.0E-33	3.1E+00	2.5E-01	1.1E-08	-1.9E+00	2.8E-01
AKR1C1_199	6.1E-14	1.6E+00	2.0E-01	1.5E-07	-1.3E+00	2.0E-01
AKR1C2_28246	1.0E-16	2.1E+00	2.4E-01	6.1E-04	-1.2E+00	2.5E-01
AKR1C3_26820	1.2E-08	1.3E+00	2.1E-01	4.3E-04	-1.0E+00	2.1E-01
AMPD3_16428	1.1E-07	1.9E+00	3.2E-01	8.9E-03	-1.7E+00	4.4E-01
ARG2_19025	1.1E-04	6.9E-01	1.5E-01	2.1E-05	-8.2E-01	1.5E-01
B3GNT3_22416	1.6E-10	2.1E+00	3.0E-01	1.5E-02	-1.3E+00	3.5E-01
CDA_11848	6.1E-14	1.9E+00	2.4E-01	2.1E-04	-1.3E+00	2.7E-01
CTSB_23180	1.1E-10	7.7E-01	1.1E-01	3.6E-03	-4.4E-01	1.1E-01
CYP24A1_11891	7.3E-20	1.9E+00	2.0E-01	1.9E-11	-1.5E+00	2.0E-01
DUSP18_15067	1.8E-03	9.1E-01	2.3E-01	1.9E-02	-9.2E-01	2.6E-01
DUSP5_24241	8.6E-06	1.4E+00	2.8E-01	8.5E-04	-1.4E+00	3.0E-01
FILIP1L_12646	3.9E-05	8.9E-01	1.8E-01	2.4E-02	-6.5E-01	1.8E-01
GCLM_2615	2.0E-16	1.5E+00	1.7E-01	2.8E-05	-9.0E-01	1.7E-01
GCNT2_20683	3.4E-02	6.3E-01	2.2E-01	3.0E-02	-7.5E-01	2.2E-01
GDF15_2621	8.9E-06	1.1E+00	2.0E-01	2.3E-02	-7.3E-01	2.1E-01
GPX2_2766	2.3E-02	1.0E+00	3.4E-01	3.4E-04	-1.6E+00	3.4E-01
MVP_4379	4.3E-06	1.5E+00	2.8E-01	2.4E-02	-1.2E+00	3.3E-01
NDRG4_14331	1.2E-11	1.8E+00	2.5E-01	2.7E-02	-9.8E-01	2.8E-01
NOS3_4638	2.5E-06	1.9E+00	3.4E-01	7.4E-04	-2.2E+00	4.8E-01
NQO1_26473	2.8E-13	1.2E+00	1.5E-01	1.2E-09	-1.1E+00	1.5E-01
PLXND1_10528	7.1E-03	5.4E-01	1.5E-01	2.2E-03	-6.7E-01	1.6E-01
RGS3_27783	1.5E-10	9.3E-01	1.3E-01	5.1E-03	-5.3E-01	1.3E-01
RNF8_15649	2.9E-03	6.8E-01	1.8E-01	1.7E-02	-6.6E-01	1.8E-01
S100A11_23914	3.4E-11	1.6E+00	2.2E-01	1.5E-03	-9.9E-01	2.2E-01
SAT1_6103	1.7E-12	1.6E+00	2.0E-01	8.5E-03	-7.8E-01	2.0E-01
SH3BGRL3_12496	5.4E-05	1.0E+00	2.1E-01	1.2E-02	-8.1E-01	2.2E-01
SLC7A11_14100	1.8E-07	1.7E+00	2.9E-01	2.6E-02	-1.2E+00	3.4E-01
SPATS2L_12688	1.8E-02	4.9E-01	1.5E-01	2.9E-02	-5.3E-01	1.5E-01
SPINT1_13261	3.4E-10	2.2E+00	3.1E-01	1.1E-02	-1.2E+00	3.2E-01
SPP1_6720	2.6E-17	1.8E+00	2.0E-01	1.5E-19	-1.9E+00	2.0E-01
TGIF1_27951	7.5E-07	6.7E-01	1.2E-01	1.7E-02	-4.3E-01	1.2E-01
TIMP1_13877	8.0E-06	1.1E+00	2.0E-01	2.6E-02	-7.1E-01	2.1E-01
TMEM45B_11590	1.4E-02	1.2E+00	3.7E-01	4.0E-03	-1.9E+00	4.5E-01
UGDH_7525	1.0E-05	1.1E+00	2.1E-01	6.1E-03	-8.2E-01	2.1E-01

**Supplemental Table 3. Common 20 genes of siKEAP1 downregulated genes/ siNFE2L2 upregulated genes and effects of Nrf2 pathway enhancing and inhibiting microRNAs.**

Probe_ID	siKEAP1			siNFE2L2		
	padj	log2FC	lfcSE	padj	log2FC	lfcSE
A1BG_25586	6.6E-05	-1.0E+00	2.1E-01	1.5E-14	1.6E+00	1.9E-01
ACSM2A_20941	4.4E-03	-8.1E-01	2.2E-01	1.9E-55	3.3E+00	2.0E-01
ALB_217	1.1E-04	-5.0E-01	1.1E-01	9.9E-23	1.1E+00	1.1E-01
APOH_21123	2.1E-02	-6.7E-01	2.2E-01	2.6E-02	7.3E-01	2.1E-01
C3_886	4.5E-07	-6.6E-01	1.1E-01	4.3E-04	5.3E-01	1.1E-01
CYP3A7-CYP3AP1_24430	3.1E-03	-6.7E-01	1.8E-01	8.7E-06	8.8E-01	1.6E-01
FABP1_11582	1.8E-02	-7.1E-01	2.3E-01	2.1E-04	1.1E+00	2.2E-01
FBXO4_21873	8.7E-04	-5.7E-01	1.4E-01	9.8E-03	5.0E-01	1.3E-01
FGB_2397	4.3E-03	-4.7E-01	1.3E-01	1.3E-03	5.6E-01	1.3E-01
HMGCR_3029	8.4E-09	-9.9E-01	1.5E-01	1.2E-03	6.5E-01	1.5E-01
IDH3A_15224	3.6E-02	-3.0E-01	1.0E-01	2.9E-02	3.5E-01	1.0E-01
IGF2_3255	3.2E-05	-1.2E+00	2.3E-01	3.0E-04	1.1E+00	2.2E-01
LEAP2_28319	8.1E-10	-1.7E+00	2.5E-01	1.3E-05	1.2E+00	2.2E-01
MBL2_16596	2.0E-02	-5.6E-01	1.8E-01	4.8E-06	9.3E-01	1.6E-01
NFATC2_12248	1.7E-06	-1.3E+00	2.4E-01	9.8E-03	7.9E-01	2.1E-01
ONECUT1_4810	4.2E-03	-1.7E+00	4.7E-01	3.6E-02	1.1E+00	3.2E-01
PAQR9_18440	1.6E-02	-4.8E-01	1.5E-01	3.7E-03	5.5E-01	1.3E-01
PECR_27673	2.1E-04	-7.5E-01	1.7E-01	6.8E-03	5.9E-01	1.5E-01
SLC30A10_20231	1.6E-08	-1.1E+00	1.6E-01	1.5E-07	9.8E-01	1.5E-01
TMEM97_7217	2.7E-02	-3.6E-01	1.2E-01	2.6E-03	5.0E-01	1.2E-01

**Supplemental Table 4. 397 overlapping genes between the common genes of the 4 Top enhancing microRNAs and siKEAP1.**

TOP2A	GCLC	DSCC1	HIST1H3F	APOA5	KIF15	MYL9
AP1S1	GCLM	KLF12	SPAG5	RAB5B	KLF6	TMEM214
ATP6V0C	GOT1	MPP7	RAB2B	FOXF2	RPS27L	HPX
DEPDC1B	HMG2	SH3BGRL3	CCDC150	SPDL1	MCM6	
FHL2	HNRNP	FILIP1L	SDCBP	TROAP	ANG	
FOSL1	HSPB8	SPATS2L	RAD23B	CTSB	ARHGAP11A	
HIST1H1C	CXCL8	CAPN2	IL6R	APOBEC3F	ASAP2	
HIST1H2BC	LOC728554	KCTD21	CLIP1	ACSL5	ATXN7L1	
HIST1H2BM	MAP2K1	AP1S3	SUSD1	PSMB9	C18orf32	
HIST1H4E	MAPK13	NCF2	HIST1H2BD	NCAPH2	CHMP1B	
HIST1H4J	MASTL	TMEM59L	SH3RF1	MTMR10	EID3	
LRP10	MLLT11	RBM39	ESYT2	RTKN2	FYTTD1	
SPC25	MMP3	CSDC2	PPP2R5B	BATF	LMNB1	
TMSB10	MOB1B	ABHD2	DNAJC18	FGG	MICAL1	
ALDH4A1	NQO1	GCNT3	TFR2	BUB1	MYL12B	
LURAP1L	NUP35	IQCJ-SCHIP1	PAQR9	DUSP1	SHB	
MCL1	PEG10	BORA	WDR45	DUSP5	TUBGCP3	
NDRG1	PSRC1	SRSF2	DHFR	CCDC138	GADD45A	
PNN	RAB5A	MND1	DTL	PIP4K2C	MSH6	
PRNP	RAD51	HECA	KLB	SLC26A1	NDC1	
S100P	RIT1	EPHA1	CYP2S1	CYP3A7-CYP3AP1	NTN4	
SASS6	RPS6	GLIPR1	MLXIPL	FHL3	PCYT2	
SKP2	RRM2	ZWILCH	ZFAND5	OPTN	ESAM	
ABCG2	S100A6	NRCAM	PALLD	KIF2A	EMC3	
NR1I2	SAT1	GIN54	EMP3	ANKRD1	CD63	
CDA	SERPINE1	CHPF	PANX1	IDS	C19orf33	
OSGIN1	SERPINE2	KANK4	ARG2	TMOD1	PPM1H	
TMC7	SH3KBP1	KIF20B	ZNF280A	TGIF1	TEP1	
YWHAZ	SLC6A14	GLUD2	HIST1H4D	SUV39H2	RBP1	
TMSB4X	SLC7A11	KIF3A	SLC16A6	VEGFB	SLC40A1	
ANXA2P2	SQSTM1	RMND1	GAB2	PTPN3	ZNF714	
CDT1	TCFL5	CREB5	LRCH1	HPN	ACSM2A	
CENPU	TDP2	C4orf32	KRT15	RCN1	HELLS	
NCEH1	TERF2IP	RALBP1	MSH2	SYT11	SERPINA4	
ANLN	TMEM97	KIAA0430	GPAM	SRPX2	B3GNT3	
SDC4	TRIB1	TM4SF19	SERPINB8	RTN4	AKAP12	

SRXN1	TXNRD1	LGALS3	OIP5	NAV3	CENPI
NR1H4	VMP1	IQCC	GLUL	MIS18A	SLC16A5
PAH	YPEL5	CENPQ	KIF3C	AGR2	FLNA
PBK	MYOF	ZDHH18	KLHL4	MAP2	MAX
AMPD3	C1QBP	DUSP18	QSOX1	CDC42EP2	EIF5A2
BIRC3	EFCAB11	MIXL1	PFKP	SKA1	STBD1
BCL2L11	GPAT3	ASAH2	SLC30A10	TPM4	C3ORF52
CASP1	KRT19	MAP1LC3B	MCCC1	AKR1C3	THOC3
CASP8	PIGA	SNRPF	KLRK1	CCNDBP1	HIST2H3A
DEPDC1	IGFBP1	ONECUT1	IDH1	CYP24A1	CLIP4
FLNB	ZNF331	PARBPB	NEK2	RELL1	NPIPA1
KIAA1217	TSNAX	MGST2	KLF5	A1BG	AKR1C1
LMO7	SECTM1	RP2	CADM1	AGTR1	IER3
NBPF15	SLC7A9	ATP9A	ASPH	MCTP1	RFC5
RRAS2	F2RL2	SEPHS1	KLC1	AGXT	COL26A1
ABCC2	SERPINC1	MMP14	GSR	S100A3	DFNA5
ABCC3	PIK3R2	RAB30	IGFBP2	ACTR3	NSMF
ANXA1	RGS10	CAP2	DGKK	DSTN	ADD3
ANXA2	C1orf109	NASP	INHBB	HNRNPA1	HMGCS2
ANXA3	GBE1	CTPS1	FBXL2	PCK1	SLC25A32
ARL6IP5	HIST1H4B	MRPL1	SEPT10	GSTA1	BACE1
ATAD5	HIST1H4F	ZC3H13	PTGR1	PDLIM3	FAM111A
ATP10D	FABP1	SLC13A5	FBXO4	SMIM24	BDH2
ATP6V1D	TMPO	ZCCHC14	XPR1	IL1R2	IDH3A
AURKA	HIST1H3A	CLIC1	ATAD2	ALB	STMN3
BID	HIST2H3D	VRK1	SLAIN2	C1orf131	ITIH1
CCNB1	SMIM14	GBP3	CENPN	CCNA2	BMF
CCNB2	HARS	TLR6	EAF2	CD3D	ACO1
DLGAP5	GINS1	ZBTB10	TAF13	CENPW	RBP2
EGR1	HIST1H2BB	RPL22L1	AGPAT5	EGF	REEP2
FGB	KLRC2	TNS4	RRP15	HMGCR	ADGRD1
FN1	NFATC2	ADAM9	SMOX	IQGAP1	SLC6A11

Metadata online on request

Supplemental Table 5. 24 overlapping genes between the common genes of the 4 top inhibiting microRNAs and siNFE2L2.

Probe_ID	siNFE2L2			miR-502-5p			miR-200a-5p			miR-363-3p			miR-25-3p		
	padj	log2FC	lfcSE	padj	log2FC	lfcSE	padj	log2FC	lfcSE	padj	log2FC	lfcSE	padj	log2FC	lfcSE
ACO1_20595	0.03	0.50	0.14	0.01	0.67	0.20	0.01	0.61	0.18	0.04	0.51	0.18	0.04	0.48	0.18
ADD3_16935	0.01	0.44	0.12	0.00	-0.66	0.18	0.00	1.50	0.14	0.00	1.01	0.14	0.00	0.90	0.14
ADGRD1_25401	0.00	2.68	0.63	0.01	2.59	0.76	0.03	2.21	0.73	0.00	3.79	0.67	0.00	5.67	0.66
BACE1_13077	0.05	0.57	0.18	0.00	0.88	0.23	0.00	1.08	0.21	0.02	0.64	0.20	0.00	0.96	0.21
BDH2_14883	0.00	0.67	0.12	0.00	1.18	0.16	0.00	1.62	0.14	0.00	0.62	0.14	0.00	0.52	0.14
BMF_16921	0.03	1.16	0.33	0.01	1.53	0.43	0.00	2.87	0.37	0.00	2.78	0.75	0.00	3.22	0.36
BMF_26899							0.03	2.32	0.77	0.00	3.17	0.36	0.01	2.42	0.76
FAM111A_13619	0.02	1.05	0.29	0.01	1.36	0.39	0.04	1.04	0.35	0.00	1.28	0.34	0.00	1.66	0.34
FRMD4B_12533	0.03	0.68	0.19	0.00	1.37	0.24	0.00	1.12	0.23	0.01	0.77	0.22	0.03	0.67	0.23
GDF15_2621	0.02	-0.73	0.21	0.03	-0.83	0.29	0.00	-1.49	0.27	0.00	-0.98	0.25	0.00	-1.39	0.26
GDF15_18329							0.00	-1.19	0.27				0.00	-1.02	0.27
HMGCS2_16503	0.00	2.75	0.44	0.00	3.89	0.55	0.00	2.33	0.52	0.00	2.61	0.50	0.00	3.20	0.50
HPX_25984	0.01	1.02	0.26	0.00	1.85	0.34	0.01	1.08	0.31	0.00	1.36	0.30	0.00	1.64	0.30
IDH3A_15224	0.03	0.35	0.10	0.00	-0.60	0.14	0.01	-0.43	0.13	0.03	-0.37	0.12	0.00	-0.67	0.13
ITIH1_16511	0.00	1.64	0.25	0.00	1.89	0.34	0.00	2.52	0.29	0.01	1.05	0.30	0.04	0.83	0.31
LEAP2_28319	0.00	1.22	0.22	0.00	1.44	0.31	0.00	1.38	0.27	0.00	-1.46	0.28	0.00	-1.78	0.29
MYL9_4413	0.01	1.25	0.33	0.04	1.20	0.44	0.00	1.53	0.39	0.04	1.10	0.39	0.00	2.16	0.38
NSMF_4729	0.02	-0.52	0.14	0.00	-0.75	0.20	0.00	-1.46	0.18	0.00	-1.05	0.17	0.00	-1.72	0.18
NSMF_14995										0.01	-1.52	0.45			
RBP2_22383	0.00	1.65	0.40	0.00	2.34	0.50	0.00	2.41	0.45	0.00	2.29	0.44	0.02	1.38	0.47
REEP2_24279	0.04	0.64	0.20	0.00	1.51	0.27	0.01	0.84	0.24	0.00	1.85	0.23	0.00	2.19	0.23
SLC25A32_6403	0.01	-0.56	0.15	0.01	-0.69	0.21	0.00	-0.73	0.19	0.00	-0.96	0.19	0.00	-1.49	0.19
SLC6A11_26630	0.03	0.49	0.15	0.03	-0.59	0.21	0.00	-0.80	0.18	0.00	-1.32	0.18	0.00	-1.32	0.18
SPP1_6720	0.00	-1.94	0.20	0.00	1.01	0.28	0.00	-0.99	0.24	0.00	-1.50	0.24	0.00	-1.44	0.24
STMN3_15411	0.00	0.99	0.22	0.01	-1.14	0.33	0.00	1.38	0.27	0.00	1.45	0.27	0.00	1.73	0.27
TMEM214_24547	0.04	0.41	0.12	0.00	-0.95	0.18	0.00	-0.68	0.15	0.00	-0.71	0.15	0.00	-1.05	0.16
TRO_7352	0.05	0.91	0.28	0.00	2.05	0.35	0.03	1.02	0.34	0.00	1.41	0.32	0.00	1.87	0.32
TRO_28012				0.05	2.81	1.05				0.04	2.30	0.80	0.02	2.79	0.95
TRO_26673				0.00	3.16	0.88							0.01	2.72	0.80

